Machine learning-constrained projection of bivariate hydrological drought magnitudes and socioeconomic risks

Rutong Liu[1], Jiabo Yin[1*], Louise Slater[2], Shengyu Kang[1], Yuanhang Yang[1], Pan Liu[1], Jiali Guo[3,4], Xihui Gu[5], Xiang Zhang[6], Aliaksandr Volchak[7]

[1]State Key Laboratory of Water Resources Engineering and Management, Wuhan University, Wuhan, Hubei, 430072, P.R. China

[2]School of Geography and the Environment, University of Oxford, Oxford, UK

[3]Engineering Research Center of Eco-environment in Three Gorges Reservoir Region, Ministry of Education, China Three Gorges University, Yichang, Hubei 443002, China

[4]College of Hydraulic and Environmental Engineering, China Three Gorges University, Yichang, Hubei 443002, China

[5]School of Environmental Studies, China University of Geosciences, Wuhan 430074, China

[6]National Engineering Research Center of Geographic Information System, School of Geography and Information Engineering, China University of Geosciences, Wuhan 430074, China

[7]Engineering Systems and Ecology Faculty, Brest State Technical University, Moskovskaya 267, 224017 Brest, Belarus

*Correspondence: Jiabo Yin (jboyn@whu.edu.cn)

21   **Abstract**

22   Climate change accelerates the water cycle and alters the spatiotemporal distribution of hydrological

23   variables, thus complicating the projection of future streamflow and hydrological droughts. Although

24   machine learning is increasingly employed for hydrological simulations, few studies have used it to project

25   hydrological droughts, not to mention the bivariate risks of drought duration and severity as well as their

26   socioeconomic effects under climate change. We developed a cascade modeling chain to project future

27   bivariate hydrological drought characteristics in 179 catchments over China, using 5 bias-corrected GCM

28   outputs under three shared socioeconomic pathways, five hydrological models and a deep learning model.

29   We quantified the contribution of various meteorological variables to daily streamflow by using a random

30   forest model, then employ terrestrial water storage anomalies and a standardized runoff index to evaluate

31   recent changes in hydrologic drought. Subsequently, we constructed a bivariate framework to jointly model

32   drought duration and severity by using Copula functions and the most likely realization method. Finally, we

33   used this framework to project future risks of hydrological droughts as well as associated exposure of gross

34   domestic product and population. Results showed that our hybrid hydrological-deep learning model

35   achieved >0.8 Kling-Gupta efficiency in 161 out of 179 catchments. By the late 21st century, bivariate drought

36   risk is projected to double over 60% of catchments, mainly located in Southwest China. Our hybrid model

37   also projected substantial GDP and population exposures by increasing bivariate drought risks, suggesting

38   an urgent need to design climate mitigation strategies toward a sustainable development pathway.

1 Introduction

In a warming world, the acceleration of the global water cycle is expected to alter the regional and seasonal distribution of key hydrological variables such as precipitation and evapotranspiration (Allan et al., 2020). As precipitation patterns are particularly sensitive to changes in atmospheric forcing and local conditions, precipitation extremes are generally increasing globally, exacerbating spatial heterogeneity of precipitation (Donat et al., 2016; Tabari, 2020). A suite of Shared Socioeconomic Pathways (SSPs) has been proposed to simulate different possible future scenarios of social responses to climate change, and these are employed to investigate the possible effects of long-term climate change (Meinshausen et al., 2020; Zhang et al., 2021). By using the SSP framework, numerous works have indicated that the redistribution of precipitation may lead to the decline of water storage in some regions, and intensify water scarcity in arid regions (Sönmez and Kale, 2018; Woolway et al., 2020; Yao et al., 2023). Under increasing atmospheric greenhouse gases, numerous studies have reported a widespread increase in drought events, even in areas with increasing annual runoff (Dai et al., 2018). The uneven distribution of precipitation and other meteorological elements under climate change complicates predictions of future runoff and drought.

China's socioeconomic development, particularly its agricultural sector, is threatened by the rapid intensification of extreme hazards under climate change (Piao et al., 2010). Over the past years, China has been hit by severe drought events which have caused considerable damage to ecosystem productivity and socio-economic growth (Zhai and Zou, 2005; Yin et al., 2023). For instance, one extreme drought in Sichuan Province in 2022 resulted in power shortages and led to economic losses of 669 million dollars. Water shortage is also a key challenge that hinders the sustainable development of the North China Plain (Chen and Yang, 2013). Over the period of 1985-2014, drought accounted for about 19% of economic losses among all meteorological hazards (Chen and Sun, 2019). With continuing global warming, the economic losses from severe drought events might increase by over ten billion US dollars per year by the late 21st century, underscoring the importance of projecting future droughts over China (Lu et al., 2023).

Droughts can be triggered by divergent mechanisms, and are thus distinguished according to the type of drought, such as meteorological and hydrological drought (Yihdego et al., 2019). The majority of studies have focused on meteorological droughts, which can then be translated to a hydrological drought, while fewer works have focused on hydrological drought probably due to a lack of measurements like the standardized runoff index (SRI) (Barker et al., 2016; Kumar et al., 2016; Tirivarombo et al., 2018). Furthermore, hydrological droughts are not only affected by the water cycle but also by human interventions, which makes them difficult to accurately be predicted (Wu et al., 2021). Currently, the majority of drought impact assessments focus on the investigation of individual drought variables (i.e., drought duration, severity and intensity, etc.) through univariate probabilistic models and stochastic theory (Myronidis et al., 2018; Byakatonda et al., 2018; Zhang et al., 2022). However, univariate drought analysis cannot accurately describe the probability of drought events, because droughts of either long duration or severe intensity can lead to

74   substantial socio-ecosystem damages (Castle et al., 2014; Udall and Overpeck, 2017). Therefore, the bivariate
75   framework based on Copula functions has been developed for drought projection, compensating for the
76   incompleteness of a single variable analysis (Ayantobo et al., 2017; Nabaei et al., 2019). At present, studies
77   on hydrological drought within a bivariate framework are still lacking. Beyond the choice of approach
78   (univariate or bivariate), the Gravity Recovery and Climate Experiment (GRACE) and GRACE-FO (GRACE
79   Follow-On) satellites now provide two decades of large-scale terrestrial water storage (TWS) data, which
80   captures the water deficit in various forms on land and can be used to monitor droughts (Schmidt et al., 2006).
81   The drought severity index based on TWS (TWS-DSI) can be used to monitor past drought events, which
82   also shows potential advantages in drought warning, forecasting, and projection (Nie et al., 2018; Pokhrel et
83   al., 2021).

84   In recent decades, many studies have used bias-corrected outputs from Global Climate Models (GCMs)
85   to project future hydrological drought scenarios (e.g., (Ashrafi et al., 2020; Kim et al., 2021; Dixit et al.,
86   2022). The growing application of machine learning has revealed a high potential for improving the accuracy
87   of hydrological simulation and prediction (Mokhtar et al., 2021). In recent years, many machine learning
88   algorithms have been adopted in drought simulation and produce good performance, such as wavelet neural
89   networks (WNNs) (Xiujia et al., 2022), support vector machines (SVMs) (Zhu et al., 2021) and long short-
90   term memory neural networks (LSTMs) (Dikshit et al., 2021a)). These algorithms can be used to simulate
91   the evolution of future droughts and construct risk maps for drought contingency planning (Rahmati et al.,
92   2020). Among the different models, the LSTMs can effectively simulate short-term and long-term streamflow
93   series, and their performances have been validated at short temporal scales (Dikshit et al., 2021b; Kang et al.,
94   2023).

95   In this study, we projected changes in bivariate hydrological drought characteristics (duration and
96   severity) and their associated socioeconomic risks under three SSPs (i.e., SSP1-26, SSP3-70, and SSP5-85)
97   over 179 catchments in China. To achieve this, we combined five hydrological models and a deep learning
98   model (i.e., the LSTM), and then drove the hybrid models with the five bias-corrected GCMs outputs under
99   Coupled Model Intercomparison Project phase six (CMIP6). Then, we employed a machine learning-based
100 framework (i.e., Random Forest, RF model) to quantify the sensitivity of different meteorological variables
101 to daily streamflow. We employed the run theory and two drought metrics, the SRI and TWS-DSI, to identify
102 and explore recent changes in drought characteristics. In addition, we used Copula functions to build the
103 bivariate model of drought duration and severity during both reference and future periods. After identifying
104 shifts in bivariate drought characteristics based on the most likely realization approach, we projected the
105 exposure of gross domestic product (GDP) and population to increasing drought risks in the future. Finally,
106 we decomposed the uncertainties arising from different sources by employing the multivariate analysis of
107 variance (MANOVA) method. This study illustrated the used materials and methods in Section 2 and Section
108 3, respectively. We compared SRI and TWS-DSI in assessing drought conditions in Section 4.1. The
109 contribution of meteorological factors to simulate streamflow and the calibration of hybrid terrestrial models
110 were shown in Section 4.2. The evolution of univariate droughts was projected in Section 4.3. The bivariate

111 droughts of future scenarios and associated socioeconomic exposures were evaluated in Section 4.4. We
112 discussed the uncertainty of our analysis and main limitations of this study in Section 5, and finally
113 summarized our work in Section 6.

114 **2. Methodology**

115   The workflow of this study is divided into four modules (Figure 1), described briefly below and detailed
116 in the following sections. In step 1, the hydrological models and LSTM are trained using the ERA5-Land
117 dataset, and then the output of HMs is used as input to feed the LSTM, thus we build the hybrid terrestrial
118 models (HTMs). In step 2, the trained HTMs are validated using in situ streamflow observations, then driven
119 by using the outputs of five GCMs from the CMIP6 to project streamflow and the SRI series. In step 3,
120 monthly drought characteristics (i.e., drought duration and severity) are defined using run theory and
121 combined with Copula functions to construct a bivariate drought framework. Future bivariate drought change
122 is evaluated using the most likely realization method. Meanwhile, the TWS measurements from GRACE
123 missions are also employed to characterize recent changes in TWS-based droughts, which are also compared
124 with the hydrological droughts. In step 4, we employ future scenarios of GDP and population alongside our
125 future drought projections to produce a socioeconomic assessment of drought exposure over China. Finally,
126 we examine the contribution of uncertainty from different sources in projecting drought change and exposure.
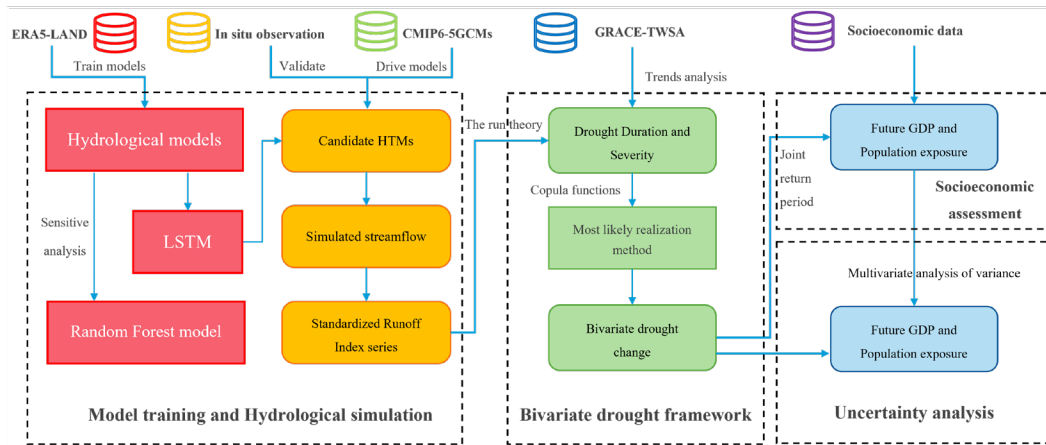
127

128 **Figure 1. Schematic flowchart of the method, including ML-constrained hydrological simulations, evaluation of**
129 **bivariate hydrologic drought characteristics and change, and the socioeconomic evaluation to drought exposure**
130 **under climate change.**

131 **2.1 Derivation of 2-meter relative and specific humidity**

132   The Clausius–Clapeyron relationship is used to derive saturated vapor pressure (e_s) and air temperature
133 (T), and is expressed as follows (Koutsoyiannis, 2012):

134
$$e_s(T) = e_0 \exp\left[(\frac{1}{T_0} - \frac{1}{T}) \frac{L_0}{R_0} \right]$$
(1)

135 where T_0, e_0, L_0 and R_0 are constants, with a value of 273.16 K, 611 Pa, 2.5×10⁶ J kg⁻¹, 461 J kg⁻¹ K⁻¹,

136 respectively;

137 Since near-surface relative humidity (*RH*) can't be directly obtained from the ERA5-Land dataset, the

138 2m temperature (T_{2m}) and dew-point temperature (T_d) are substituted into equation (1) to calculate *RH*:

$$RH = \frac{e_s(T_d)}{e_s(T_{2m})} = \exp\left[(\frac{1}{T_{2m}} - \frac{1}{T_d})\frac{L_0}{R_0}\right] \tag{2}$$

140 Then, the near-surface air pressure (*ps*) and T_d are used to deduce the specific humidity (*SH*), which is

141 mathematically expressed as follows (Simmons et al., 1999):

$$SH = \frac{0.622 \times e_s(T_d)}{ps - 0.378 e_s(T_d)} \tag{3}$$

2.2 Sensitivity analysis on meteorological variables for runoff

144 The RF model is used to calculate the sensitivity to different meteorological variables for runoff,

145 including precipitation (*pr*), air pressure (*ps*), surface downwelling shortwave and longwave radiation (*srsds*

146 *and srlds*), *RH*, *SH,* average temperature, maximum and minimum temperature. The contribution of a key

147 variable is derived by using the pre-established model, the perturbed meteorological variable and remaining

148 (non-perturbed) variables (Antoniadis et al., 2021; Green et al., 2020). The percentage change in streamflow

149 is derived from the following equation:

$$S_i = \frac{\text{mean}\left(R_{(i+1\text{SD})} - R_{(all)}\right)}{\text{stdev}\left(R_{obs}\right)} \times 100\% \tag{4}$$

151 where S_i indicates the sensitivity of streamflow to i^{th} meteorological variable, which are *pr*, *ps*, *SH*, *RH*, *srlds*,

152 *srsds* and temperature; R_{obs} is the observation of streamflow which has units of m³/s; $R_{(i+1SD)}$ is the simulated

153 streamflow by perturbing *i* by +1 SD; $R_{(all)}$ is the streamflow simulated by all meteorological variables; stdev

154 (R_{obs}) represents the standard deviation of $R_{obs.}$

2.3 Deep learning-constrained hydrological modeling

2.3.1 Conceptual hydrological models

157 For preliminary hydrological simulations, we select five hydrological models to represent hydrological

158 characteristics under different environments. The GR4J (Génie Rural à 4 paramètres Journalier) is a lumped

159 model with 4 parameters developed by Perrin et al. (2003). GR4J consists of two water store modules (runoff

160 yielding and routing) and uses daily rainfall and evapotranspiration as inputs to simulate streamflow series

161 (Kunnath-Poovakka and Eldho, 2019). This model has been successfully used to simulate hybrid runoff

162 processes on many continents (Shin and Kim, 2021; Gu et al., 2023). Additionally, we use the temperature-

163 based method (Oudin et al., 2005) to estimate the potential evapotranspiration of the GR4J model.

164   The HBV (Hydrologiska Byråns Vattenbalansavdelning) model was initially developed by the Swedish

165   Meteorological and Hydrological Institute for Hydrological Forecasting (BERGSTRÖM and FORSMAN,

166   1973). This model includes five modules and one transform function to quantify hydrological variables (i.e.,

167   precipitation, snow, soil moisture, runoff, baseflow) (Bergström, 1995). It has been widely employed to

168   simulate streamflow, and it particularly has a good capacity for simulating snowmelt runoff (Kriauciuniene

169   et al., 2013).

170   The HMETS (hydrological model of École de technologie supérieure) model contains 21 parameters

171   and two reservoirs (i.e., the saturated and vadose zones), which makes it simplified and efficient to complete

172   hydrological simulation (Martel et al., 2017). The model can simulate six processes in water cycle, including

173   the accumulation, melts and refreezing of snow, water infiltration and routing, and evapotranspiration (Qi et

174   al., 2020). It has been growly used for streamflow simulation under climate change and has shown great

175   performance (Chen et al., 2018).

176   The SIMHYD (simple lumped conceptual daily rainfall-runoff) model is a daily rainfall-runoff model

177   developed by Porter and McMahon (1975). There are four types of runoff from different sources: impervious

178   areas, infiltration, interflow, and groundwater storage (Chiew et al., 2002). Although the model was

179   developed earlier, it has shown good accuracy in simulating runoff over China (Yu and Zhu, 2015).

180   The XAJ (Xinanjiang) model is a hydrological model, which can usually achieve better performance in

181   humid and semi-humid areas than in arid areas (Ren-Jun, 1992). As the model was developed based on the

182   underlying surface of the Yangtze River Basin in China, it is composed of a three-layer evapotranspiration

183   module with four parameters and separates the runoff into four components (i.e., surface water, groundwater,

184   interflow water and flow routing) (Tian et al., 2013). To date, it is widely reported that the XAJ model usually

185   shows the best accuracy in simulating hydrological conditions in China (Hu et al., 2005). However, due to

186   inadequacies in the simulation of arid regions, the results of the XAJ model did not be considered as the best

187   option in northern China.

188   We use the SCE-UA (Shuffled Complex Evolution) approach to maximize the objective function (i.e.,

189   Kling-Gupta efficiency) to optimize these models (Duan et al., 1992). The most complete 20-year observation

190   period is selected to calibrate five models in each watershed. To calibrate the hydrological models, a cross-

191   validation method developed by Arsenault et al. (2017) is used for calibration, which employs the odd years

192   of data to calibrate models, and the even years of data to validate. As catchments are located in different

193   climatic regions, the parameters of models are calibrated for each catchment, which means that the parameters

194   are not universal. Although uncertainties shown by hydrological models are ineradicable, the overall

195   uncertainty is acceptable in the current scale after optimizing five hydrological models for each catchment.

196   **2.3.2 Hybrid scheme of hydrological model and machine learning**

197   Recurrent neural network (RNN) models have had considerable success in hydrological modeling (Cho

198   et al., 2014; Sherstinsky, 2020). However, when considering long input sequences, RNNs struggle to capture

199   the relationships between distant points due to a phenomenon known as "long-term dependencies" (Yu et al.,

200   2019). With the development of deep learning, this problem can be successfully avoided by using LSTMs.

201   An LSTM cell includes input, output and forget gates. The input gate determines which new information

202   can be stored in the cell state, and the forget gate identifies which information will be discarded from the cell

203   state. The output gate controls what part of the cell state is selected as the output. The updated cell state is a

204   combination of the information retailed and the new information to be added. By using this architecture, the

205   LSTM can avoid the problem of gradient vanishing or explosion during backpropagation, especially when a

206   series is long (Gers et al., 2000). The LSTM can be expressed as follows:

207
$$fg_t = \sigma(W_{hf} hs_{t-1} + W_{xf} x_t + b_f) \tag{5}$$

208
$$ig_t = \sigma(W_{hi} hs_{t-1} + W_{xi} x_t + b_{fg}) \tag{6}$$

209
$$\tilde{c}_t = \tanh(W_{h\tilde{c}} hs_{t-1} + W_{xc} x_t + b_{\tilde{c}}) \tag{7}$$

210
$$c_t = fg_t \cdot c_{t-1} + ig_t \cdot \tilde{c}_t \tag{8}$$

211
$$og_t = \sigma(W_{oh} hs_{t-1} + W_{ox} x_t + b_o) \tag{9}$$

212
$$hs_t = og_t \odot \tanh(c_t) \tag{10}$$

213   where x_t, fg_t, ig_t and og_t are input variables, and forget, input and output gates at time t, respectively; W_i,

214   $W_{\tilde{c}}$, W_f and W_o are the weights of each gate; the operator '$\odot$' is the symbol for the dot product of two vectors;

215   c_t and hs_t are the cell state of the LSTM and the hidden unit at the time t, c_{t-1} and hs_{t-1} at the former time

216   $t-1$; $\tilde{c}_t$ is the activation function of hidden layer; b_i, b_f, b_o and b_c are bias itemsand the; $\sigma(\cdot)$ and $\tanh(\cdot)$

217   are the sigmoid function and the hyperbolic tangent function, respectively; at the initial moment, cell and

218   hidden states are set to zero arrays.

219   The hydrological outputs together with other climate variables are used as inputs to feed the LSTM

220   model (i.e., the HMs are thus constrained by the LSTM). Because changes in meteorological variables require

221   some time to converge before they are reflected in the runoff, it is essential to calculate the lag time caused

222   by the flow convergence for the model. The catchment response lag time d is defined as the time during

223   which precipitation accumulates in the river to generate runoff for the gauge downstream, and is

224   mathematically expressed as follows (Berne et al., 2004; Ganguli and Merz, 2019):

225
$$d = 2.51 A_d^{0.4} [\text{ hrs }] = 0.11 A_d^{0.4} [\text{ days }] \tag{11}$$

226   where A_d (km^2) represents the catchment area; meteorological variables from day T-d to day T are employed

227   to drive HTMs.

228   We combine the five hydrological models with LSTM to construct five HTMs. To compare the

229   performance of the HTMs, we use ten HTMs as candidates for streamflow simulation in each catchment. The

230   calibrated HTMs are then driven by the outputs of five GCMs under each SSP (aggregated to produce a basin

231 average series) during 1985-2100 over 179 catchments to project future daily streamflow.

2.4 Drought indexes and run theory

233 The TWS-DSI is employed to measure the degree of terrestrial drought severity (Zhao et al., 2017). It
234 is a dimensionless standardized water storage anomaly index, which can indicate terrestrial drought
235 conditions when below the mean standard value. The TWS-DSI can be mathematically expressed as follows:

$$TWS\text{-}DSI_{x,y} = (TWS_{x,y} - \overline{TWS_y})/\sigma_y \tag{12}$$

237 where $TWS_{x,y}$ is the TWS at year x and month y; $\overline{TWSA_y}$ and σ_y represent the means and standard deviation

238 of TWS at month y, respectively.

239 The SRI is a measure of the variability of runoff for a given duration based on the percentage of
240 accumulated runoff. (Shukla and Wood, 2008). The hydrological drought classification and ranges indicated
241 by SRI are shown in Table S1. To calculate the SRI, we simulate the retrospective time series of streamflow
242 and fit the sample series to a probability distribution. The SRI is considered to follow a Pearson type-III
243 distribution (Vicente-Serrano et al., 2012), and is calculated as follows:

$$SRI = \begin{cases} -(r - \dfrac{c_0 + c_1 r + c_2 r^2}{1 + d_1 r + d_2 r^2 + d_3 r^3}) & 0 < F(x) \le 0.5 \\[4mm] r - \dfrac{c_0 + c_1 r + c_2 r^2}{1 + d_1 r + d_2 r^2 + d_3 r^3} & 0.5 < F(x) \le 1 \end{cases} \tag{13}$$

245 where $r = \sqrt{\ln\left[\dfrac{1}{F(x)^2}\right]}$; $F(x)$ is the cumulative probability density of SRI; c_0, c_1, c_2, d_1, d_2 and d_3 are

246 the empirical constants, taken as 2.516, 0.803, 0.010, 1.433, 0.189, 0.001, separately.

247 After calculating the two drought indexes, the degree of water deficit can be determined according to
248 the Grades of Meteorological Drought and the previous classification (Dikici, 2020). Table S1 presents the
249 drought classification and thresholds used for identifying drought degrees. The run theory is employed to
250 obtain characteristics of drought events from the time series (Yevjevich, 1967). When the drought index is
251 below the mild drought (i.e., ≤-0.5 drought index), a drought event is detected (Figure 2), and then the drought
252 duration and drought severity are extracted.
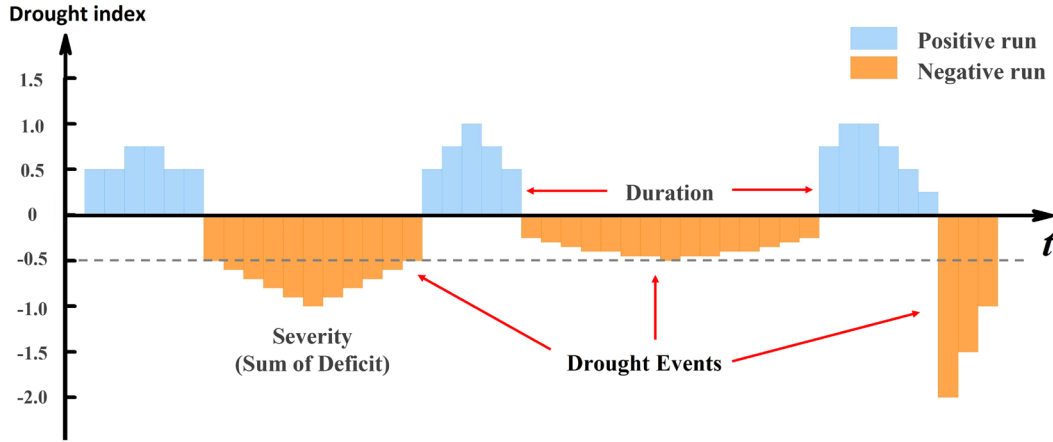
253

254 **Figure 2. Drought duration and severity identification based on run theory, where -0.5 denotes the drought**
255 **threshold (grey dash line).**

256 **2.5 Socioeconomic exposure assessments based on the Copulas and most likely realization**

257 After extracting the drought duration (D) and severity (S), we fit their marginal distributions with seven

258 distributions shown in Table S2. The OR case (i.e., a bivariate drought event is identified with either a high

259 severity or long duration) of the joint return period (JRP) under a Copula-based framework is used to quantify

260 the occurrence of drought events (Yin et al., 2020). The joint distribution of drought duration and severity is

261 constructed by using a Copula function, which is valuable for describing correlated hydrological variables

262 (Li, 1999). Unlike univariate drought frequency analysis, the JRP within a bivariate framework can be

263 represented by an isoline, which contains infinite combinations of multivariate variables. It is important for

264 risk assessments to select a representative combination along the isoline. Previous studies have typically

265 selected joint design values according to the same frequency hypothesis, but this approach lacks a statistical

266 basis and poorly describes the physical characteristics of droughts (Yin et al., 2018). In this paper, the joint

267 probability density is used to optimize the most likely realization, which is mathematically expressed as

268 follows:

269
$$\begin{cases} (d^*, s^*) = \arg\max f(d, s) = c[F_d, F_s] \bullet f_d \bullet f_s \\ C[F_d, F_s] = 1 - \mu / T_{or} \\ c[F_d, F_s] = \dfrac{dC(F_d, F_s)}{d(F_d)d(F_s)} \end{cases} \tag{14}$$

270 where $c[F_d, F_s]$ is the Copula probability density function; f_d and f_s are the fitted probability density

271 functions of D and S, respectively; F_d and F_s are the marginal distribution of D and S, respectively; (d^*, s^*)

272 is the most likely realization under a given JRP T_{or}; μ is the mean inter-arrival time between two

273 consecutive droughts.
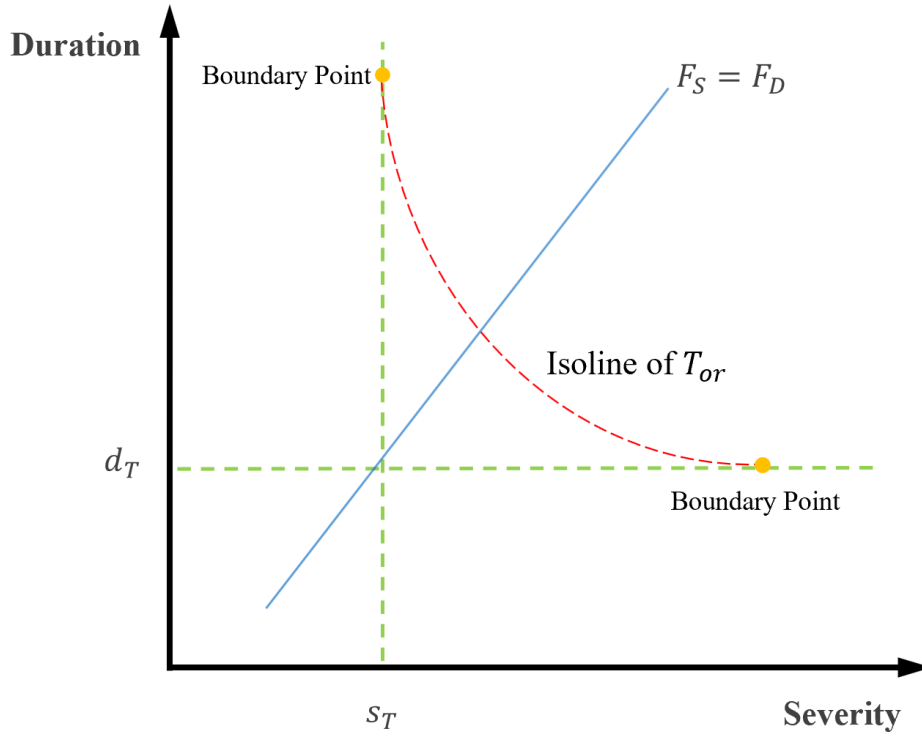
274
275 **Figure 3. Joint distribution of drought duration and severity under a critical T_{or}. The green lines are two arbitrary**
276 **values of duration and severity. The red line is the isoline line of two variables under a critical T_{or}, and the blue**
277 **line denotes the traditional equal-frequency assumption.**

278

279   Socioeconomic exposure has previously been defined as ranging from 0 to 100% in the future period

280 (Gu et al., 2020a), but dynamically shifting climate risks cannot be represented under this static definition.

281 Here, the socioeconomic exposure is defined by considering the shift in JRP, and is expressed at the catchment

282 scale as follows:

283
$$E_{POP} = \frac{T_h I(T_h - T_f)}{T_f A_d} \times POP \tag{15}$$

284
$$E_{GDP} = \frac{T_h I(T_h - T_f)}{T_f A_d} \times GDP \tag{16}$$

285 where E_{POP} and E_{GDP} denote the population and GDP exposure; T_h and T_f denote the historical and future

286 JRP, respectively; $I(\cdot)$ denotes the controlling function, which is 1 when $T_h - T_f > 0$, or 0 when $T_h - T_f \geq 0$

287 is recorded; POP (GDP) denotes the population (GDP) of a given catchment in the future climate.

288 **2.6 Quantifying the uncertainty contributed by different sources**

289   Uncertainties in the future drought projections can arise from the SSPs, GCMs and HTMs. During both

290 historical (1985-2014) and future periods (2071-2100), the combination of 3 SSPs, 5 GCMs and 10 HTMs

through the impact modeling chain resulted in 150 hybrid combinations. The overall uncertainty is calculated from the variance of the future estimated JRP relative to the historical 50-year droughts. To partition the uncertainty from different sources of data and their interaction effects, the MANOVA is used and expressed as follows (Weinfurt, 1995):

$$\Delta y_{x,y,z} = M + S_x + G_y + H_z + I_{x,y,z} \tag{17}$$

where M denotes the mean change of all indicators in models; S_x, G_y and H_z denote the impact on indicators of the xth SSP, y^{th} GCM and z^{th} HTM, respectively; $I_{i,j,k}$ is the overall impact arising from the interactions of different sources. The overall variance V is then expressed as follows:

$$V = VS + VG + VH + VI_{SG} + VI_{SH} + VI_{GH} + VI_{SGH} \tag{18}$$

where VS, VG, VH are the variance from the SSPs, GCMs and HTMs, respectively. VI_{SG}, VI_{SH}, VI_{GH} and VI_{SGH} denote the variance caused by the coupling between different sources of data. The contribution of each source to the overall uncertainty is quantified by the variance of each source by the total variance.

3. Data and materials

3.1 In situ observation dataset

We use a gridded meteorological dataset with 0.5° × 0.5° resolution, including daily temperature (maximum, minimum and average, ℃) and daily precipitation (mm) from 1961 to 2018, provided by the National Meteorological Bureau of China. The dataset is regarded as the latest gridded meteorological dataset in China and has been applied to some studies (e.g., Wu et al., 2018; Yin et al., 2021a,b). Meanwhile, we gathered the daily streamflow of 463 in situ hydrological stations spanning different periods during 1961-2018. The hydrological stations are densely distributed in East China, while West China has a sparser distribution. Through rigorous data quality checks, 179 unnested basins with at least 20 years of data are selected, covering nine major watersheds in China. For more details on streamflow data processing and catchment screening, please refer to Yin et al. (2021b).

3.2 GRACE/GRACE-FO measurements

Temporal variations in the Earth's gravitational field observed by GRACE satellites have been used to retrieve TWS data (Tapley et al., 2004). Many international institutes have released the TWS mascon products at a monthly scale, including the JPL (Jet Propulsion Laboratory of the California Institute of Technology), the GSFC (Goddard Space Flight Center of NASA), and the CSR (Center for Space Research of the University of Texas). As these three mason solutions are produced different spatial resolutions, we produce blended TWS data based on the average of JPL, GSFC and CSR with 0.5°×0.5° resolution from 2002 to 2022,

321   and fill the missing data using a linear interpolation approach (Yin et al., 2022).

322   **3.3 ERA5-Land dataset**

323   ERA5-Land is a dataset that consists of a large volume of meteorological variables, including
324   precipitation, temperature and air pressure etc. The spatial resolution of dataset is 9 km and the temporal
325   resolution is one hour (Yilmaz, 2023). Under the latest global reanalysis and the lapse rate correction, the
326   ERA5-Land reanalysis dataset provides a substitute for unavailable observed weather data, by taking the
327   effect of altitude on the spatial scheme of climate variables into consideration (Pelosi et al., 2020). Six
328   variables are used in the study (i.e., pr, ps, T_{2m}, T_{dew}, $srlds$, $srsds$) and aggregated to a daily scale from the
329   hourly scale before conducting data analysis.

330   **3.4 Bias-corrected GCM outputs and socioeconomic scenarios**

331   The climate outputs of five GCMs under historical scenario and three SSPs (i.e., SSP1-26, SSP3-70,
332   SSP5-85) under CMIP6 are used to represent climate scenarios. The series of bias-corrected variables have
333   been downscaled to $0.5° \times 0.5°$resolution from 1850 to 2100 under the Intersectoral Impact Model
334   Intercomparison Project 3b (ISIMIP3b) (Lange, 2019). To reduce the systematical biases of CMIP6 raw
335   outputs, seven variables from the bias-corrected ISMIP3b dataset have been used, namely temperature (daily
336   average, maximum and minimum), pr, ps, $srsds$, $srlds$, RH and SH.

337   Population and GDP data under three SSPs are employed to evaluate the potential socioeconomic risks
338   of drought in a warming world. An open-access population dataset is adopted which takes into consideration
339   the universal two-child policy, the census results and the statistical annual report (Jiang et al., 2017). The
340   economic index from 2010 to 2100 is estimated based on the Cobb-Douglas and Population-Environment-
341   Development model (Jiang et al., 2018). All of the data have been previously used to assess the socio-
342   economic impact of extreme hydrologic hazards (Yin et al., 2022; Yin et al., 2023).

343   **4. Results**

344   **4.1 Observed changes in SRI and TWS based drought**

345   As there are insufficient streamflow observations to compute the SRI in northwest China, we also
346   employ the TWS-DSI as a supplement. This approach enriches the variety of water storage or flux being
347   evaluated. Trends in drought characteristics (i.e., frequency, duration and severity) are estimated by using the
348   GRACE/GRACE-FO dataset and observed runoff across China. Figure 4 and Figure 5 show the drought
349   trends based on the TWS-DSI and SRI, respectively. Overall, the two indexes show similar trends in most
350   catchments, suggesting that drought hazards have increased in recent decades. TWS-DSI droughts have
351   increased in 54% of areas, which are mainly located in the Qinghai-Tibet Plateau, the North China Plain and
352   the northwestern Xinjiang Province. Likewise, SRI droughts have increased over 51% of studied catchments,
353   which mainly dominate northeastern and southeastern China. The severity of droughts measured by the

354   TWS-DSI index is twice of the hydrological drought, primarily because the TWS-DSI metric incorporates
355   all vertical water fluxes, offering a comprehensive view of shifts in water scarcity. Some locations exhibit
356   discrepancies depending on the index considered. For instance, droughts in the Qinghai-Tibet Plateau and
357   Northeast China show opposite trends. Anomalies in the Qinghai-Tibetan plateau may be explained by the
358   transformation of snowpack melt into surface runoff under the influence of climate change, which helps
359   compensate for the lack of surface water in the area (Stewart, 2009). The discrepancy observed in
360   Northeastern China could potentially be linked to the rise in soil moisture from increased infiltration, which
361   causes a higher proportion of water to be stored within the soil than at the surface, interfering with the
362   quantification of hydrological drought (Wang et al., 2017). Finally, both indicators show a consistent positive
363   drought trend in most areas of China and particularly the North China Plain and Pearl River Basin.
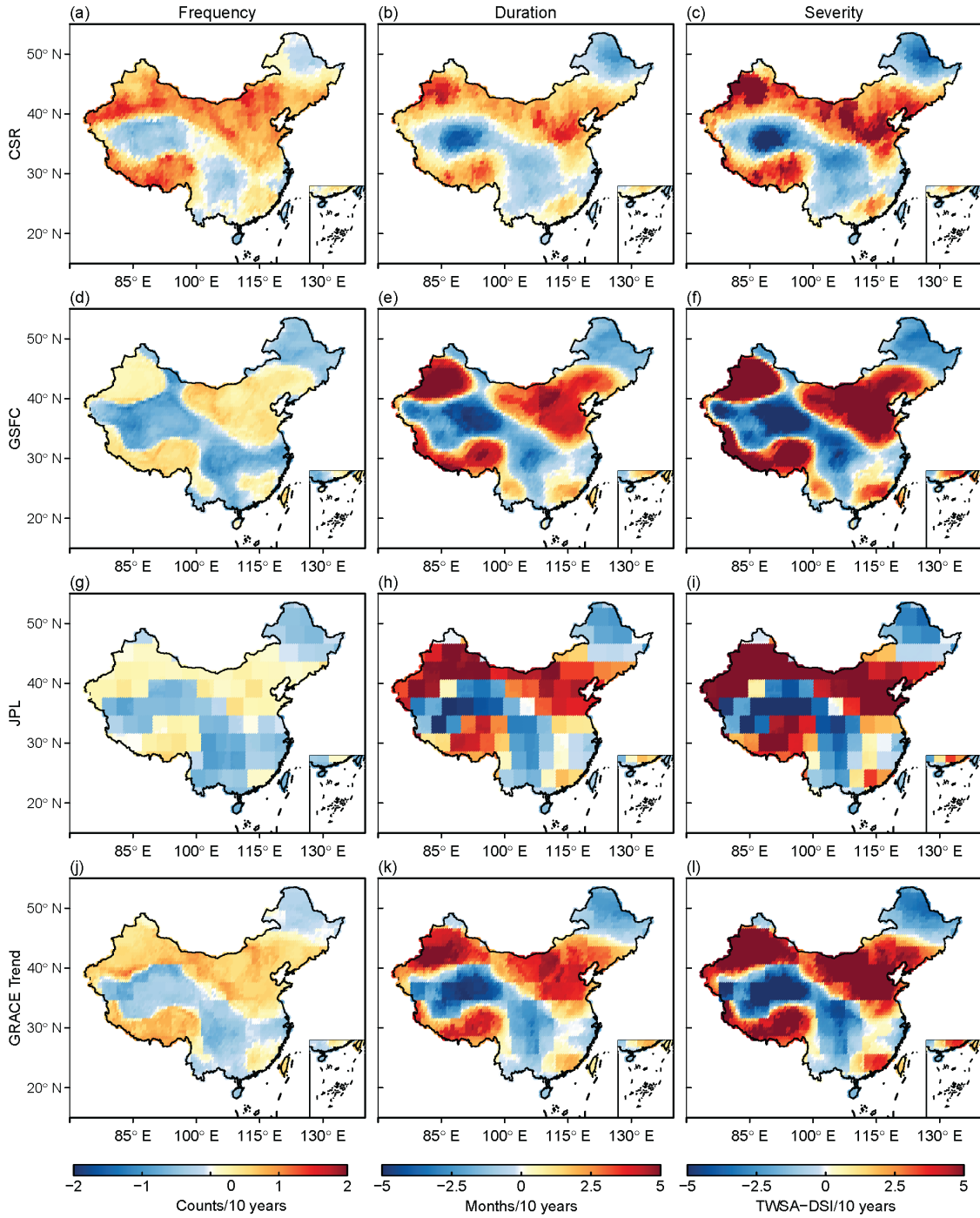
364
365 **Figure 4. Trends in drought frequency, duration and severity based on the TWS-DSI from 2002 to 2022 using**
366 **three GRACE/GRACE-FO products (a-i) and the blended data (j-l).**
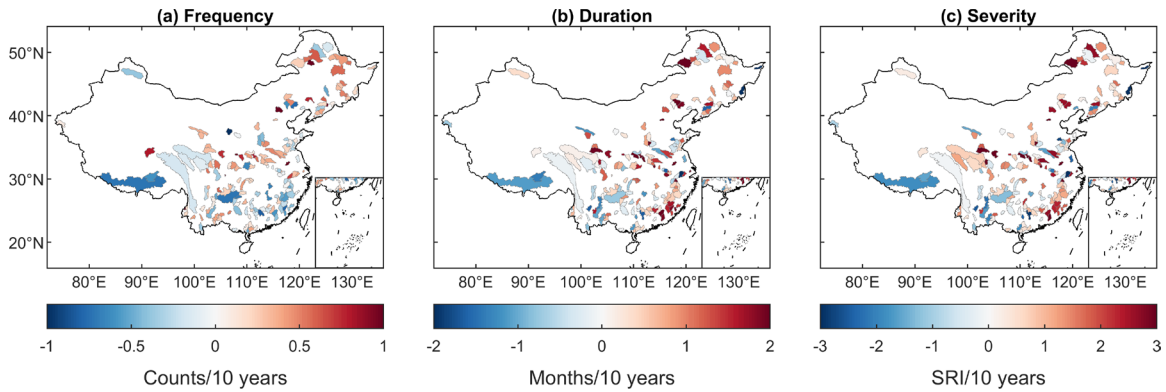
Figure 5. Trends in drought frequency, duration and severity based on SRI over China.

4.2 Machine Learning-constrained streamflow simulation and model evaluation

The RF model was used to quantify the sensitivity of streamflow to different meteorological variables (Figure 6). We quantified the sensitivity of seven historical mean meteorological variables (i.e., *pr*, *ps*, *SH*, *RH*, *srlds*, *srsds*, temperature) to monthly streamflow in each grid. Due to the sparse number of observation stations in Northwestern China, the reliability of the sensitivity analysis for these regions is lower than that of the dense observed areas. Precipitation typically plays a major role in generating runoff in Southeast China, although *SH* plays the most important role in some regions such as Central, Southwest and Northeast China. Over 30% and 38% of stations show a sensitivity rate of >10% in Western and Northeastern China, respectively. In contrast, *RH* and shortwave radiation have a negative contribution to streamflow; especially shortwave radiation, which has a pronounced negative sensitivity in 394 stations probably due to enhanced evapotranspiration (Ma et al., 2019). In general, *RH* contributes to increasing streamflow over most regions of China, but the opposite effect is observed in 179 stations mainly located in Southwestern China, Yellow River and Huaihe River basins. This is the result of the mutual feedback of water and heat dynamics (i.e., saturated vapor pressure increases with warming and intensifies evaporation, leading to a decrease in surface water), which was also found by Liu et al. (2017). The temperature has a positive contribution to streamflow generation in Northeast China, suggesting a potential mitigation for the deficiency of surface flow. However, there is interactive feedback between hydrological and thermal factors that result in an inability to directly assess the impact of temperature on hydrologic droughts.
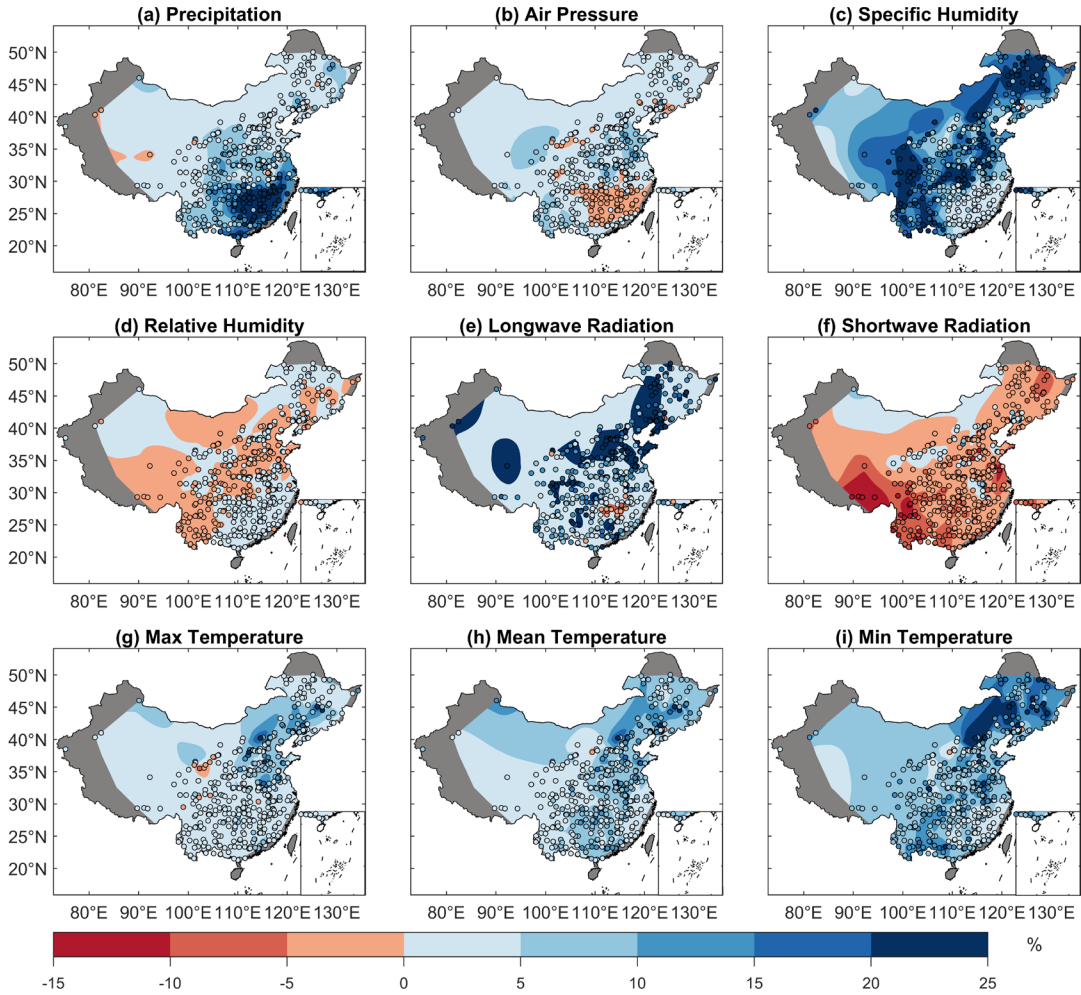
Figure 6. Sensitivity of meteorological variables to daily streamflow. The figure uses a thin plate smoothing spline method to interpolate the point-based station data (circles). Gray areas indicate missing data.

The performances of simulated streamflow by different HTMs are shown in Figure 7. The model that has the largest KGE is considered to be the best-performing in each catchment. In Fig 7. (a) and (b), the GR4J and GR4J-LSTM performed best in 77 out of 179 studied catchments. The median KGE value of GR4J is higher than 0.83, revealing a superior performance than the other hydrological models. Subsequently, the XAJ and XAJ-LSTM are the best models in 57 catchments, mainly located in the southern Yangtze River. Last, the HBV and HBV-LSTM performed best in only 10 catchments, where the streamflow are impacted by snowfall in plateaus and northern frozen areas. All catchments exhibit KGE values greater than 0.9 during the calibration period in Figure 7c, showing good performance in simulation. During the validation period, only 18 catchments have KGE values below 0.6, and most of the catchments have KGE values greater than 0.8 in Figure 7d. In summary, the trained models simulate streamflow well in all the studied catchments. Additionally, the KGE values in the southern region are generally higher than those in the northern region during the validation period, which is consistent with previous hydrological simulation works (Gu et al., 2020b, 2021). This phenomenon may be attributed to the higher dependence of streamflow on rainfall in South China, which is governed by a humid climate pattern (Zheng et al., 2022).
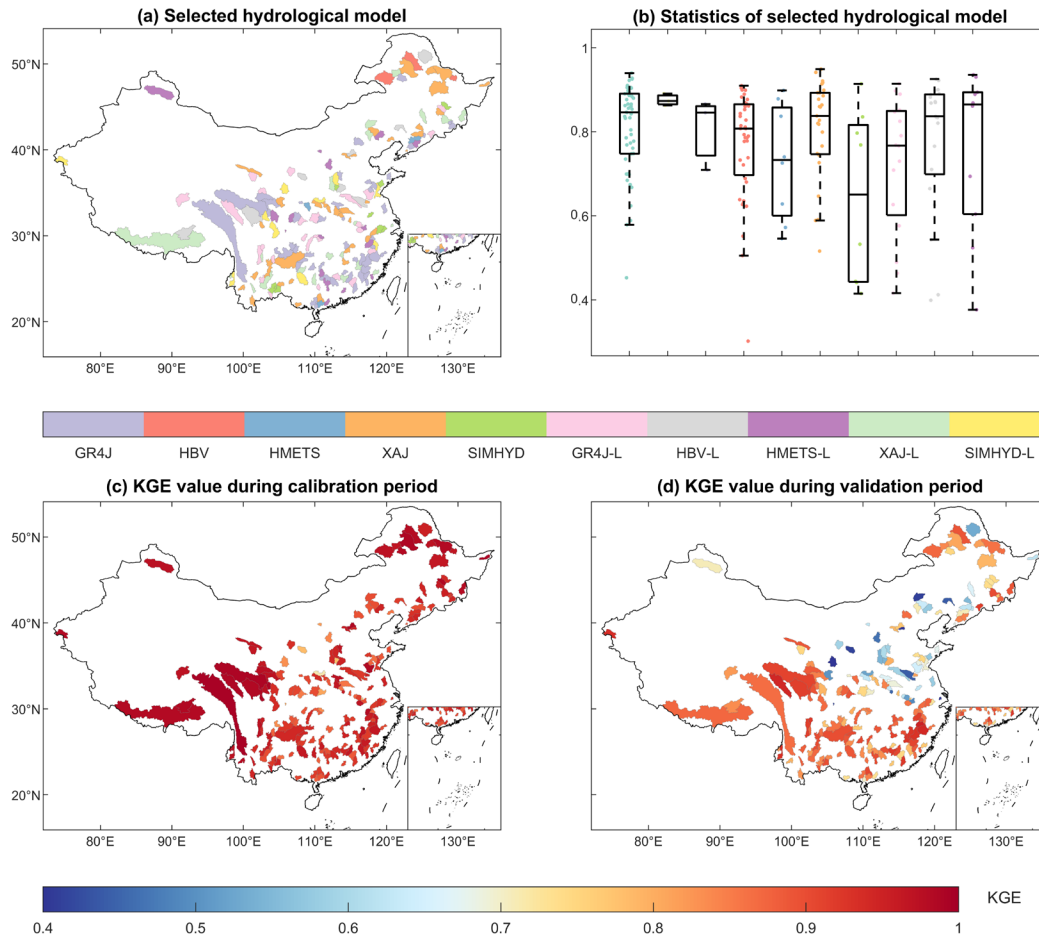
404

405 **Figure 7. Hydrological simulation performances of all candidate models. (a), The best-performing model with the**
406 **highest KGE value. (b), Boxplots of all catchments for ten HTMs indicated by KGE values. (c)-(d), The highest**
407 **KGE values during the calibration (c) and validation (d) period, respectively.**

408 **4.3 Projected changes in univariate drought characteristics**

409   We projected the future daily runoff series by driving the HTMs with the bias-corrected CMIP6 variables,

410 and then we estimated the monthly SRI to identify drought duration and severity. Based on the maximum

411 Bayesian Information Criterion (BIC), we selected the best-performing marginal distributions for duration

412 and severity from seven candidate distributions shown in Table S2, based on historical data for each

413 catchment. Figure 8 and Figure 9 show the multi-model ensemble average severity and duration for the 50-

414 year historical return period (RP).

415   In western China, we projected a significantly increasing drought trend under the three SSPs, which

416 indicates potential for increased water scarcity and more frequent extreme drought events. In Southeast China,

417 we projected that drought events are likely to intensify under SSP3-70 but not under SSP5-85. It is generally

418 considered that SSP5-85 is accompanied by higher carbon emissions than that of SSP3-70 (O'Neill et al.,

419 2016). However, future works also take significant action to control the extent of climate change combined

420 with strong climate policies under SSP5-85 (Fujimori et al., 2017). As a result, there is no deterioration of

421 drought severity with policy interventions, which emphasizes the significance of ensuring the implementation

422 of climate strategies. In northern China, in contrast, we found that future drought risks are projected to

423 decrease under the three scenarios, which is possibly related to more moisture convergence from the East

424 Asian monsoon circulation as the warming climate (Chowdary et al., 2019).
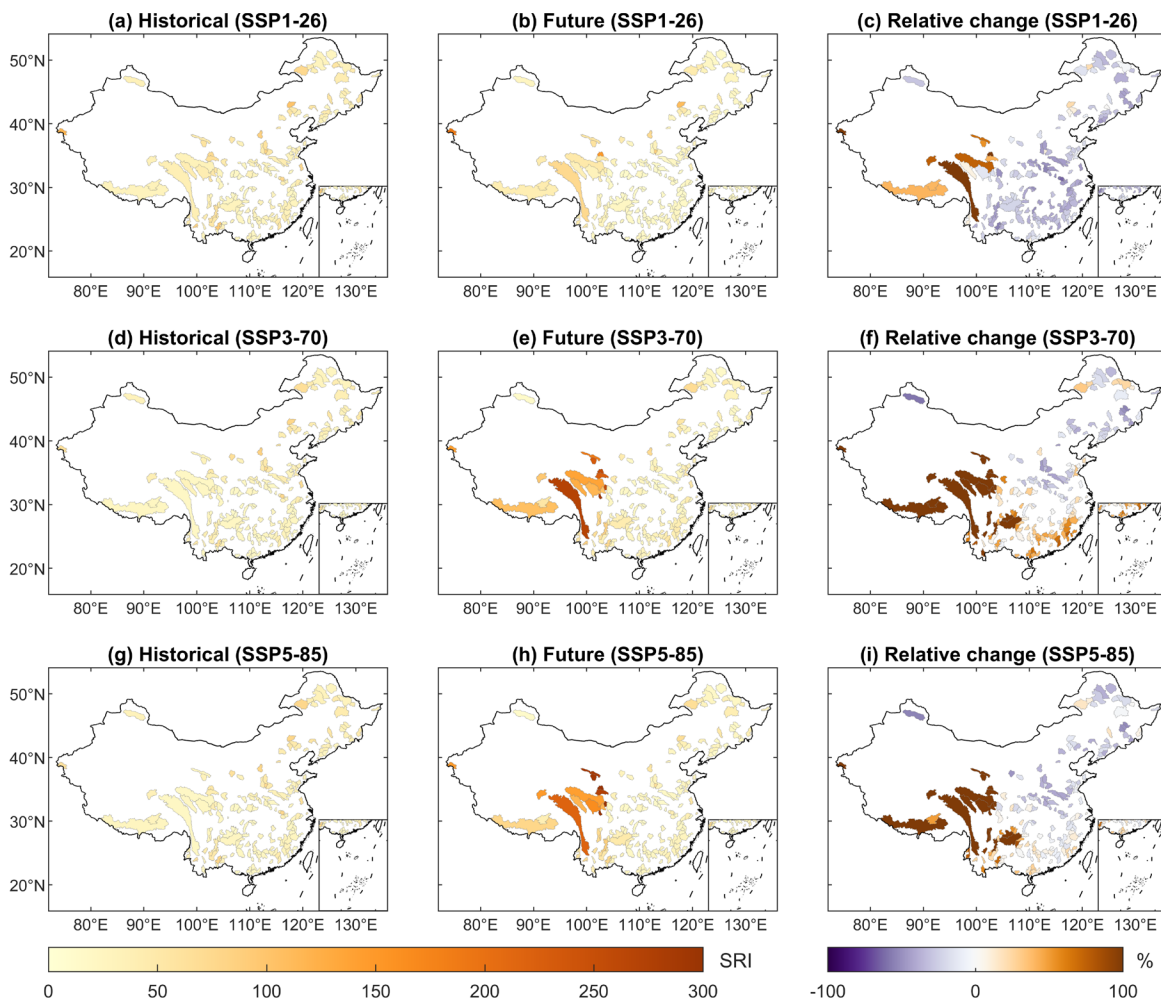
425
426 **Figure 8. Multi-model ensemble average design severity (dimensionless) under a 50-year RP for three SSPs, and**
427 **relative changes (%) in 2071-2100 compared to 1985-2014.**
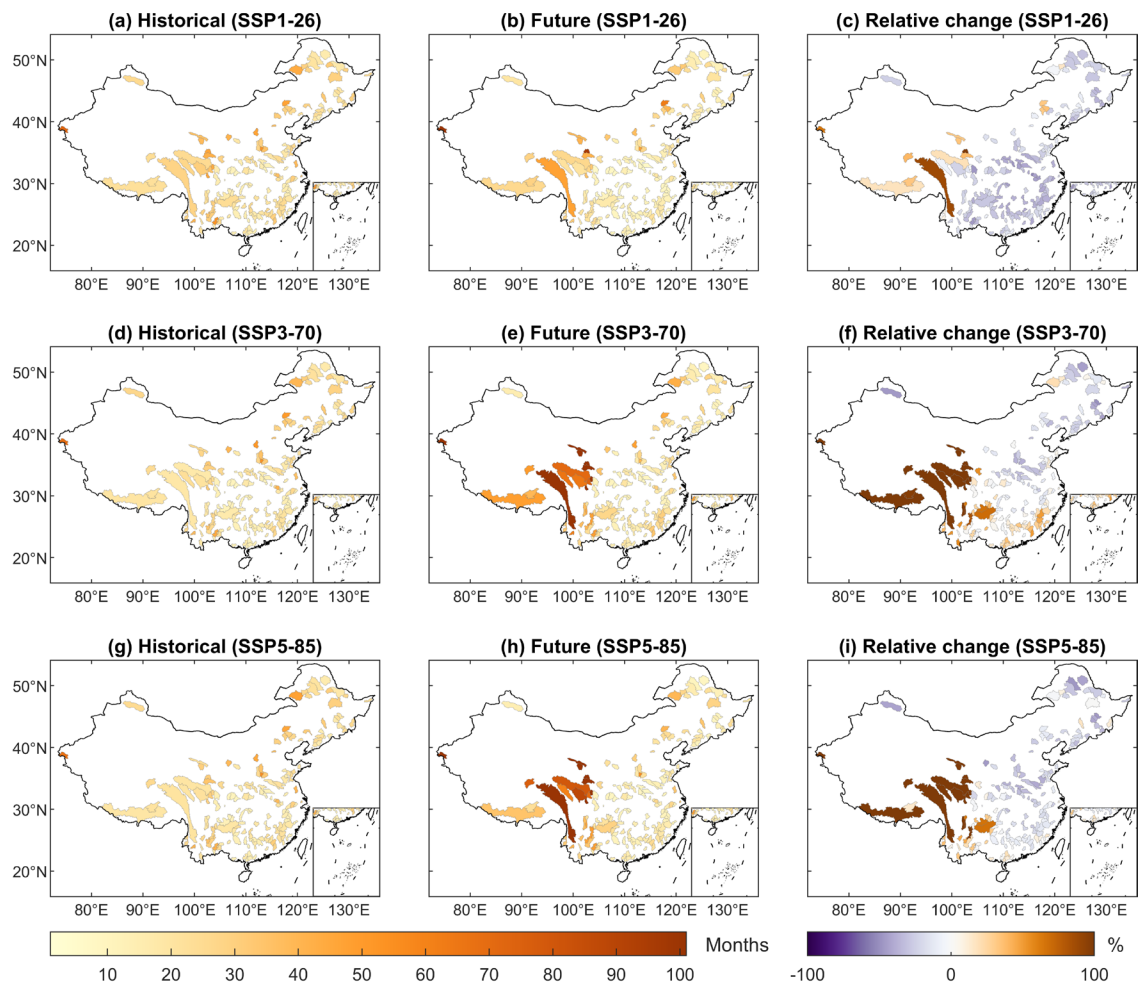
Figure 9. Multi-model ensemble average design duration (months) of the multi-model for a 50-year RP for three SSPs, and relative changes (%) in 2071-2100 compared to 1985-2014.

We display the relative change of drought characteristics under 50-year RP for all catchments for five GCMs under the three SSPs using violin plots (Figure 10). For most catchments, the relative change of drought duration and severity is negative. However, the relative change under some scenarios reached a maximum of 400%, highlighting the extreme change of drought. The median relative change of severity based on the IPSL_CM6A_LR under SSP3-70 are 30%, and 22% of catchments have a relative change over 200%, representing the most severe case of drought evolution. Furthermore, the distributions of the projections based on the MPI-ESM1-2-HR, MRI-ESM2-0 and UKESM1-0-LL models are highly skewed and bimodal under SSP3-70 and SSP5-85, revealing substantial spatial heterogeneity across China. Overall, the severity and duration of droughts slightly increase in some catchments and have the risk of extreme intensification as global warming.

M-1:GFDL-ESM4   M-2:IPSL-CM6A-LR   M-3:MPI-ESM1-2-HR
M-4:MRI-ESM2-0   M-5:UKESM1-0-LL
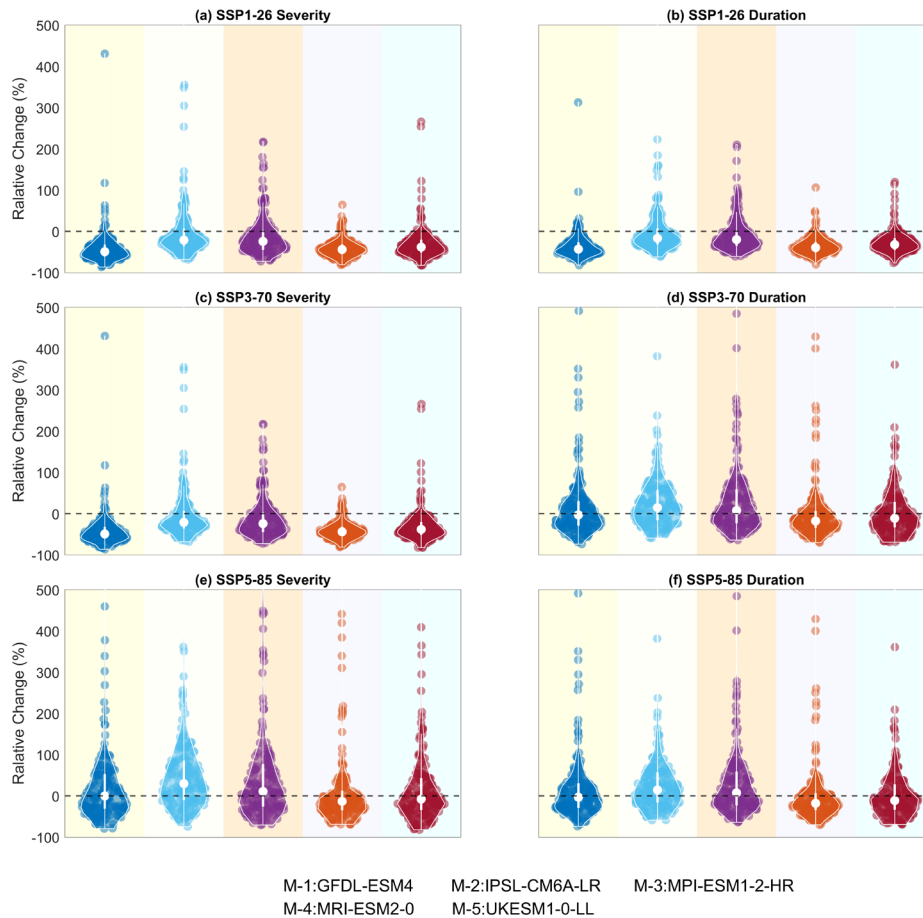
Figure 10. Violin plots of relative changes (%) in severity and duration to the historical drought event with 50-year RP under three SSPs. The white circles are the median values of relative changes.

4.4 Bivariate drought changes and corresponding socioeconomic risks

To capture the complex dependence structure between drought severity and duration, we use a Copula function to quantify the bivariate risk of hydrological droughts under climate change. Changes in the JRP of the historical (1985-2014) drought event with 50-year JRP in the future (2071-2100) period are shown in Figure 11. The medians of the projected future JRP are 38.78, 14.52 and 19.24 under SSP1-26, SSP3-70 and SSP5-85, respectively. For 69% and 60% catchments under SSP3-70 and SSP-5-85, we find the JRP of the 50-year drought is reduced to less than 25 years in the future period, suggesting that the risk of drought increases over 2 times in these catchments. Besides, we find a marked increase in the number of catchments with increased drought risk compared to the univariate drought assessments. The JRP of catchments in Northeastern and Central China tends to decrease, suggesting higher changes in risks than univariate assessments. This result is consistent with previous studies (He et al., 2011; Xu et al., 2015), which indicates that the use of bivariate drought analysis can synthesize the effects of two drought characteristics.

Future GDP and population exposed to increasing bivariate drought risk under three scenarios are shown in Figure 12. The eastern coastal regions have a higher significant economic exposure such as the Huaihe River Basin, the Yangtze River Basin and the Pearl River Basin, which is consistent with the distribution of

economically developed regions in China. The medians of GDP exposure are 5.5, 9.8 and 14.3 million dollars/km^2 under three SSPs respectively, which indicates the vulnerability of economic losses to drought disasters under global warming. The population affected by drought is mainly located in the southern Yangtze River Basin and the Huaihe River Basin under SSP3-70, as the median exposure is 525 and 205 people/km^2 under SSP3-70 and SSP5-85, respectively. This is because the increase in population is higher in the Sichuan, Guangdong and Zhejiang provinces than in other Chinese provinces under SSP3-70 (Chen et al., 2020). Overall, the exposure of GDP and population shows large heterogeneity in their sensitivity to different scenarios, and the distribution of the affected catchments is consistent with economic and social development.
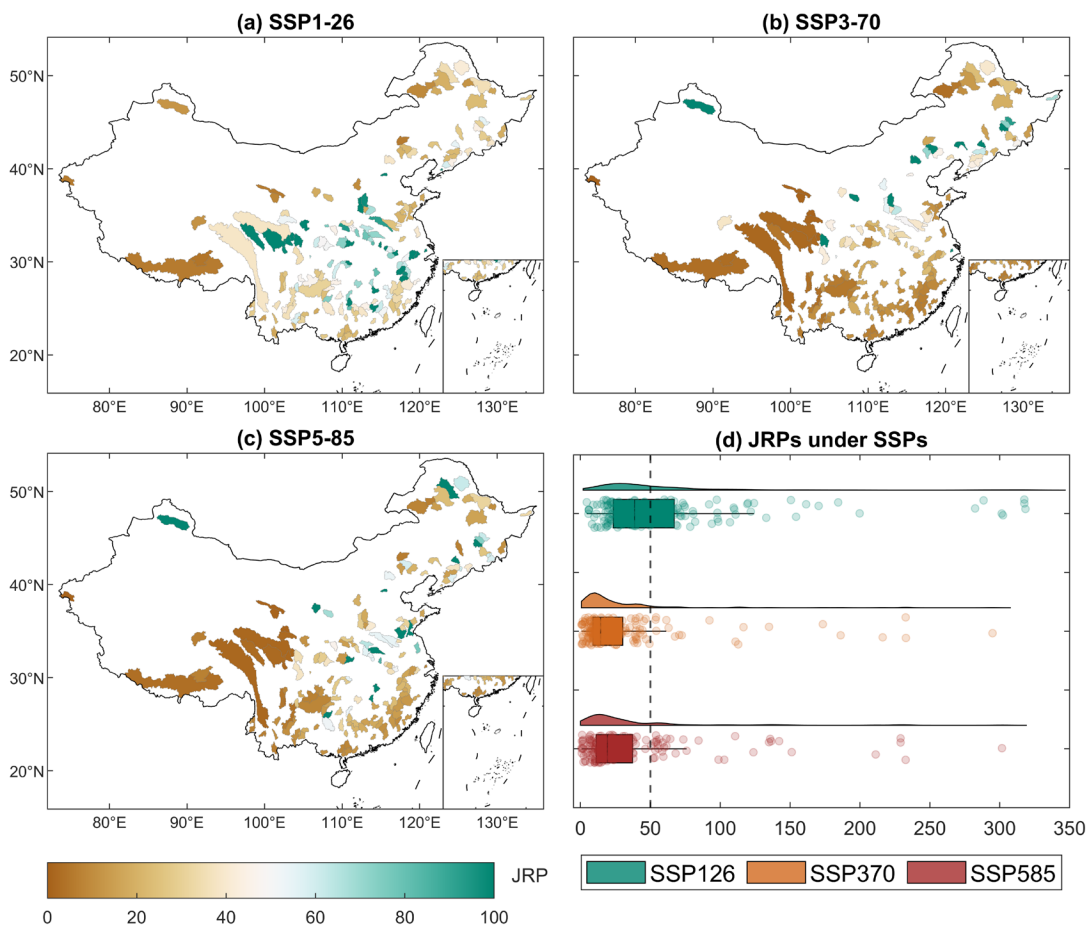
Figure 11. The future multi-model ensemble means JRP of the historical drought with a 50-year RP based on the bivariate approach. The future JRPs of 179 catchments under three SSPs are presented in (a)-(c), while (d) displays raincloud plots of the projected JRP under each SSP.
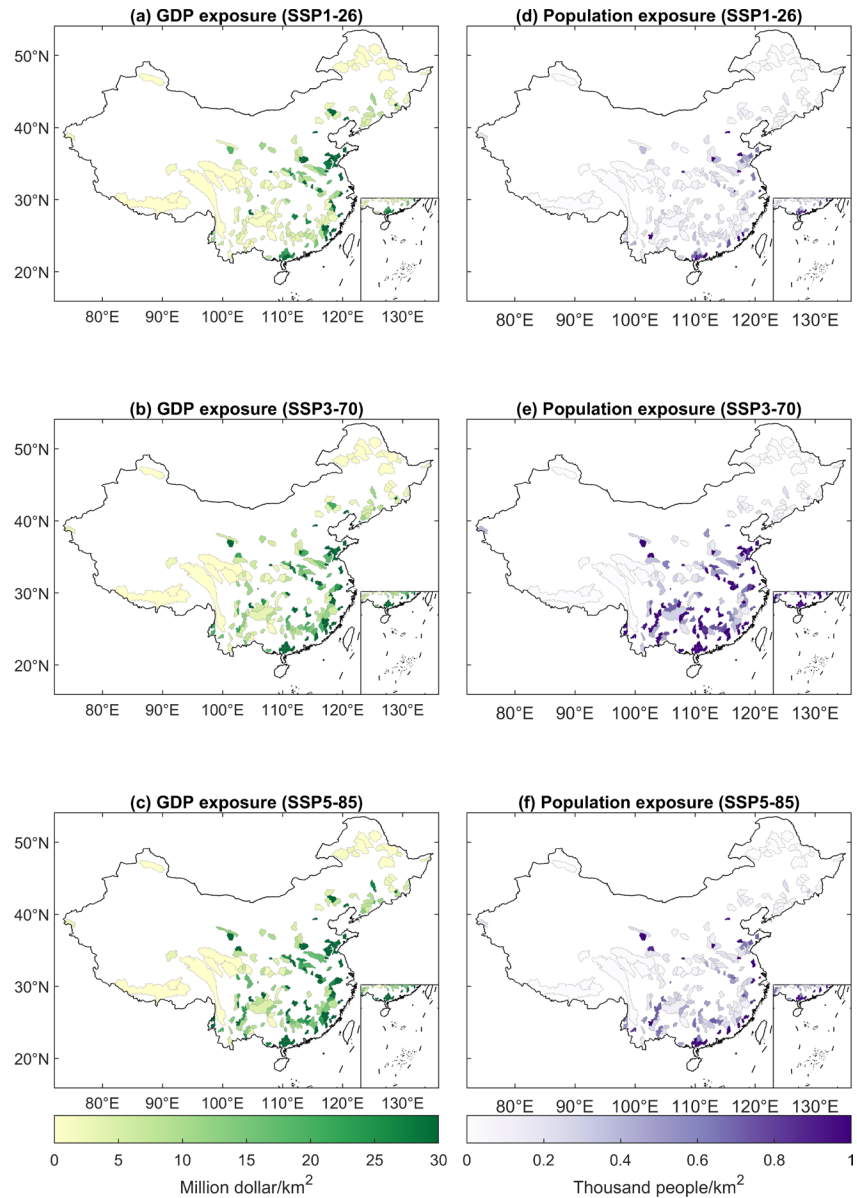
472

473 **Figure 12. The multi-model ensemble means exposure of GDP (a-c) and population (d-f) to bivariate drought**
474 **characteristics under different SSPs in the future period.**

5. Discussion

5.1 Uncertainty decomposition

The overall uncertainty in our projections arises from the different SSPs, GCMs and HTMs as well as their interactions. We assemble these seven sources using MANOVA (Figure 13). For GDP and POP exposure, we find HTM is the main source of uncertainty, and contributes 27.55% and 26.14% uncertainty, respectively. This indicates that the quality of the HTM is important for the accuracy of socioeconomic predictions. Likewise, the GCM and GCM-HTM provide over 30% of the uncertainty in GDP and population exposures,

482   which indicates the critical importance of bias-corrected GCM outputs for accurate projections. Further, the

483   contributions of the SSPs to population exposure is 1.5 times than that of GDP exposure, which shows that

484   the effect of climate change is greater for POP exposure than GDP exposure. In particular, the independent

485   factors (i.e., SSP, GCM, HTM) contribute over 50% to the uncertainty of GDP and population exposures,

486   suggesting that GDP and population exposures are less responsive to complex coupling. In contrast, the

487   coupled factors (i.e., the combination of SSP, GCM or HTM) mainly contribute to the uncertainty of the JRP,

488   accounting for 82.63% of the overall uncertainty, especially the SSM-GCM-HTM, which accounts for 36.97%

489   of uncertainty. Finally, the relatively low contribution of the choice of SSP, SSP-GCM and SSP-HTM to JRP

490   uncertainty indicates that the future risk projection uncertainty is relatively stable in future risk projections
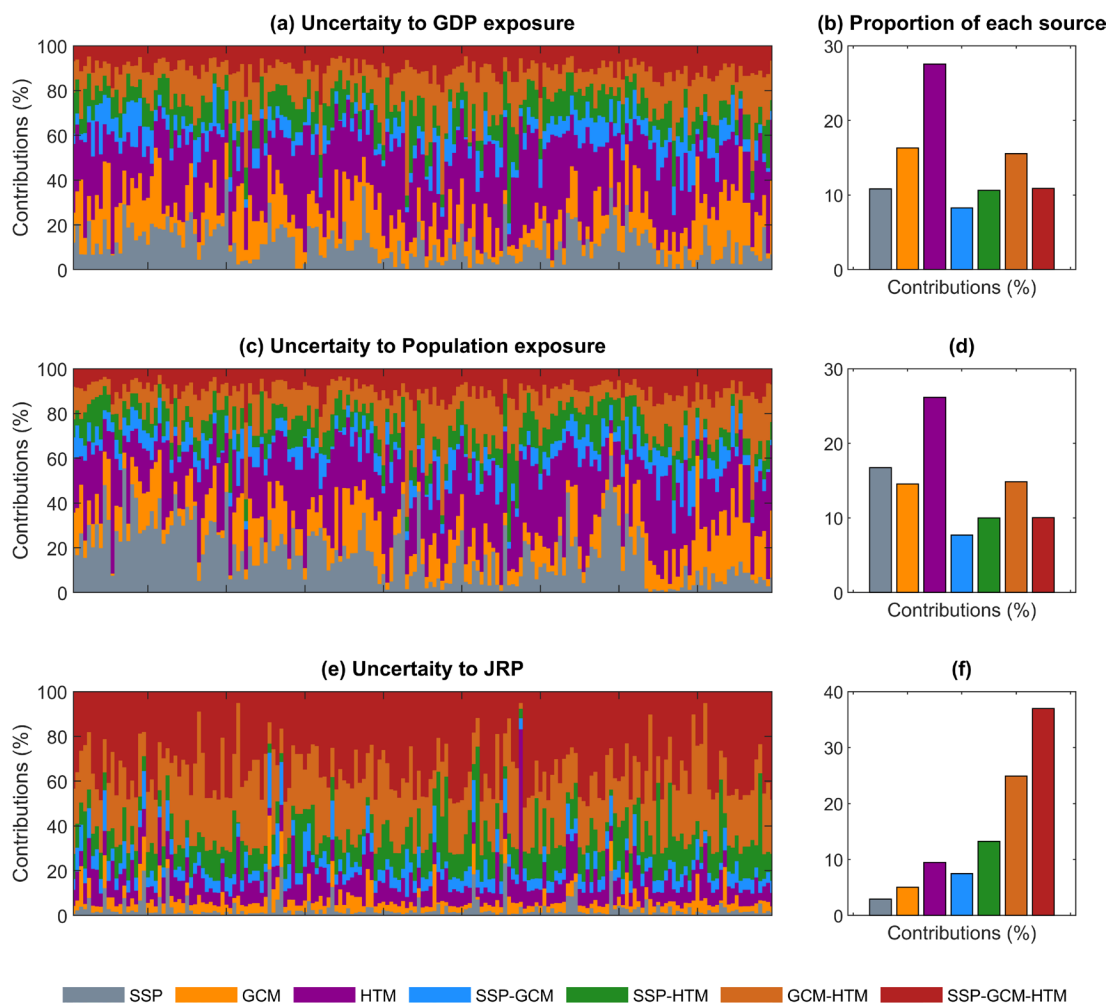
491

492   **Figure 13. The fractional uncertainty contributions of all sources to the GDP exposure, population exposure, and**
493   **JRP estimate for all 179 catchments (a, c, e) and the average fractional contribution of each source (b, d, f).**

494   **5.2 Limitations and future work**

495   The uncertainty caused by the underlying surface situation and the coupling relationships behind

496   interrelated variables remains unexplained in this study. Therefore, revealing interactions among multisource

497   data is important to understand how the drivers affect the water cycle under climate change. Here, only five

498   GCM outputs and one in situ observation dataset were used to drive our HTM models. The sparse dataset
499   may undermine the robustness of the approach. Providing a larger number of GCMs and observational data
500   to assemble a more sophisticated model might be an effective approach to improve accuracy and reliability.
501   On the other hand, due to the heterogeneity of different climatic regions in China, we would like to expand
502   hydrological models (e.g., the weather research and forecasting model hydrological modeling system, soil
503   and water assessment tool or the hydrological modules of land surface process models) to reduce uncertainty
504   in future research. Finally, the GDP and population projections cannot well reflect future economic
505   development and population migration, especially the governmental interference in immigration and
506   economic policies. It is better to consider the dynamic impact of human management on socioeconomic
507   development, which is essential for the construction of a more reliable projection framework.

508   **5.3 Suggestions for drought mitigation in China**

509   In order to curb global warming and mitigate the threats of climate change, the Chinese government is
510   striving to reach its carbon peak before 2030, achieve carbon neutrality before 2060, and bolster efforts in
511   disaster reduction (Kundzewicz et al., 2019; Liu et al., 2022b). China has nonetheless experienced several
512   extreme drought events during the past 5 years, threatening the population's health and economic
513   development (Ding and Gao, 2020; Mallapaty, 2022; Liu et al., 2022a). The Intergovernmental Panel on
514   Climate Change (IPCC) has emphasized that projections of future climate trends can equip policymakers
515   with the scientific insight needed to navigate the challenges of climate change (Pörtner et al., 2022). The
516   results of this study aim to alert policymakers to drought risk in Southwestern China which was just hit by
517   severe drought events and expected to significantly intensify with climate change. We strongly highlight the
518   importance of strictly implementing carbon emission reduction initiatives and developing prevention
519   programs to limit potential drought losses. Preserving local ecological balance and employing rational use of
520   water resources could be the key to mitigating potential losses from extreme droughts (Sohn et al., 2016;
521   Chang et al., 2019). Although China has constructed hydraulic structures with a total water storage capacity
522   of over 7,064 billion m3, current irrigation facilities need to expand to mitigate the challenge of drought
523   under climate change (Xiao-jun et al., 2012; Cai et al., 2015). In addition, it is also beneficial for
524   policymakers that establish a drought information system to get a comprehensive collection of drought
525   impacts from all potential sectors, which can link the government and research organizations (Wilhite et al.,
526   2007).

527   The Intergovernmental Panel on Climate Change (IPCC) has emphasized that projections of future
528   climate trends can equip policymakers with the scientific insight needed to navigate the challenges of climate
529   change (Pörtner et al., 2022). The results of this study aim to alert policymakers to drought risk in
530   Southwestern China, which is expected to intensify with climate change. Preserving local ecological balance
531   and employing rational use of water resources could be the key in mitigating potential losses from extreme
532   droughts (Sohn et al., 2016; Chang et al., 2019). Finally, this work highlights the importance of strictly
533   implementing carbon emission reduction initiatives and developing prevention programs to limit potential

534   drought losses.

6. Conclusions

536   In this study, the hybrid LSTM-constrained hydrological models show high accuracy in studied
537   catchments over China, demonstrating that machine learning can effectively constrain the hydrological
538   projections. Projected changes in 50-year bivariate drought characteristics, expressed as a JRP, indicate that
539   the risk of hydrological drought is likely to more than double in over 60% of catchments by the end of the
540   21st century under SSP5-85. The spatial distribution of change reveals that the catchments with severely
541   increased drought risk are mainly located in southwestern China. Notably, the exposure of GDP and
542   population varies greatly across different SSPs. The median GDP exposure under SSP5-85 is 1.5 times that
543   of SSP3-70, but the median population exposure is just 40% that of SSP3-70. The higher population exposure
544   under SSP3-70 can be attributed to rapid population growth. Finally, we find the interaction between multiple
545   sources of data explains more than 80% of the uncertainty in future changes in JRPs, showing the importance
546   of considering the relationships between model components. Our findings demonstrate that China will face
547   higher drought risks in a warmer future, emphasizing the urgency of implementing strategies to reduce carbon
548   emissions. Our study is insufficient in the revelation of drought hazard drivers and needs to expand datasets
549   and hydrological models to promote the reliability of simulation in future studies. We would also like to take
550   governmental interference of economic and demographic policies into consideration.

Data availability

The gridded meteorological dataset for China can be obtained from http://www.cma.gov.cn. The
ISIMIP3b data can be downloaded from https://data.isimip.org. The ERA5-Land data can be
downloaded from https://www.ecmwf.int/en/era5-land. Streamflow simulations used in this study
are available at https://osf.io/fvyse/.

Acknowledgments

J.Y. acknowledges support from the National Natural Science Foundation of China (Grant NOs.
52361145864; 52261145744). L.S. is supported by UKRI (MR/V022008/1). J.G. is supported by the
National Natural Science Foundation of China (NO. 52179018). This work is also supported by the
Undergraduate Training Programs for Innovation and Entrepreneurship of Wuhan University. The
numerical calculations in this paper have been performed on the supercomputing system in the
Supercomputing Center of Wuhan University.

Competing interests

At least one of the (co-)authors is a member of the editorial board of Hydrology and Earth System
Sciences.

References

Allan, R. P., Barlow, M., Byrne, M. P., Cherchi, A., Douville, H., Fowler, H. J., Gan, T. Y., Pendergrass, A. G., Rosenfeld, D., Swann, A. L. S., Wilcox, L. J., and Zolina, O.: Advances in understanding large-scale responses of the water cycle to climate change, Annals of the New York Academy of Sciences, 1472, 49–75, https://doi.org/10.1111/nyas.14337, 2020.

Antoniadis, A., Lambert-Lacroix, S., and Poggi, J.-M.: Random forests for global sensitivity analysis: A selective review, Reliability Engineering & System Safety, 206, 107312, 2021.

Arsenault, R., Essou, G. R., and Brissette, F. P.: Improving hydrological model simulations with combined multi-input and multimodel averaging frameworks, Journal of Hydrologic Engineering, 22, 04016066, 2017.

Ashrafi, S. M., Gholami, H., and Najafi, M. R.: Uncertainties in runoff projection and hydrological drought assessment over Gharesu basin under CMIP5 RCP scenarios, Journal of Water and Climate Change, 11, 145–163, 2020.

Ayantobo, O. O., Li, Y., Song, S., and Yao, N.: Spatial comparability of drought characteristics and related return periods in mainland China over 1961–2013, Journal of Hydrology, 550, 549–567, 2017.

Barker, L. J., Hannaford, J., Chiverton, A., and Svensson, C.: From meteorological to hydrological drought using standardised indicators, Hydrology and Earth System Sciences, 20, 2483–2505, 2016.

Bergström, S.: The HBV model, Computer models of watershed hydrology, 443–476, 1995.

BERGSTRÖM, S. and FORSMAN, A.: DEVELOPMENT OF A CONCEPTUAL DETERMINISTIC RAINFALL-RUNOFF MODEL, Hydrology Research, 4, 147–170, 1973.

Berne, A., Delrieu, G., Creutin, J.-D., and Obled, C.: Temporal and spatial resolution of rainfall measurements required for urban hydrology, Journal of Hydrology, 299, 166–179, 2004.

Byakatonda, J., Parida, B. P., Moalafhi, D. B., and Kenabatho, P. K.: Analysis of long term drought severity characteristics and trends across semiarid Botswana using two drought indices, Atmospheric research, 213, 492–508, 2018.

Cai, X., Zeng, R., Kang, W. H., Song, J., and Valocchi, A. J.: Strategic Planning for Drought Mitigation under Climate Change, Journal of Water Resources Planning and Management, 141, 04015004, https://doi.org/10.1061/(ASCE)WR.1943-5452.0000510, 2015.

Castle, S. L., Thomas, B. F., Reager, J. T., Rodell, M., Swenson, S. C., and Famiglietti, J. S.: Groundwater depletion during drought threatens future water security of the Colorado River Basin, Geophysical research letters, 41, 5904–5911, 2014.

Chang, J., Guo, A., Wang, Y., Ha, Y., Zhang, R., Xue, L., and Tu, Z.: Reservoir operations to mitigate drought effects with a hedging policy triggered by the drought prevention limiting water level, Water Resources Research, 55, 904–922, 2019.

Chen, H. and Sun, J.: Increased population exposure to extreme droughts in China due to 0.5 °C of additional warming, Environ. Res. Lett., 14, 064011, https://doi.org/10.1088/1748-9326/ab072e, 2019.

Chen, J., Li, C., Brissette, F. P., Chen, H., Wang, M., and Essou, G. R.: Impacts of correcting the inter-variable correlation of climate model outputs on hydrological modeling, Journal of hydrology, 560, 326–341, 2018.

Chen, Y., Guo, F., Wang, J., Cai, W., Wang, C., and Wang, K.: Provincial and gridded population projection for China under shared socioeconomic pathways from 2010 to 2100, Scientific Data, 7, 83, https://doi.org/10.1038/s41597-020-0421-y, 2020.

Chen, Z. and Yang, G.: Analysis of drought hazards in North China: distribution and interpretation, Nat Hazards, 65, 279–294, https://doi.org/10.1007/s11069-012-0358-3, 2013.

Chiew, F. H. S., Peel, M. C., and Western, A. W.: Application and testing of the simple rainfall-runoff model SIMHYD., Mathematical models of small watershed hydrology and applications, 335–367, 2002.

Cho, K., Van Merriënboer, B., Gulcehre, C., Bahdanau, D., Bougares, F., Schwenk, H., and Bengio, Y.: Learning phrase representations using RNN encoder-decoder for statistical machine translation, arXiv preprint arXiv:1406.1078, 2014.

Chowdary, J. S., Hu, K., Srinivas, G., Kosaka, Y., Wang, L., and Rao, K. K.: The Eurasian jet streams as conduits for East Asian monsoon variability, Current Climate Change Reports, 5, 233–244, 2019.

Dai, A., Zhao, T., and Chen, J.: Climate Change and Drought: a Precipitation and Evaporation Perspective, Curr Clim Change Rep, 4, 301–312, https://doi.org/10.1007/s40641-018-0101-6, 2018.

621 Dikici, M.: Drought analysis with different indices for the Asi Basin (Turkey), Sci Rep, 10, 20739,
622   https://doi.org/10.1038/s41598-020-77827-z, 2020.
623 Dikshit, A., Pradhan, B., and Huete, A.: An improved SPEI drought forecasting approach using the long
624   short-term memory neural network, Journal of environmental management, 283, 111979, 2021a.
625 Dikshit, A., Pradhan, B., and Alamri, A. M.: Long lead time drought forecasting using lagged climate
626   variables and a stacked long short-term memory model, Science of The Total Environment, 755,
627   142638, 2021b.
628 Ding, T. and Gao, H.: The record-breaking extreme drought in Yunnan Province, Southwest China during
629   spring-early summer of 2019 and possible causes, Journal of Meteorological Research, 34, 997–1012,
630   2020.
631 Dixit, S., Atla, B. M., and Jayakumar, K. V.: Evolution and drought hazard mapping of future
632   meteorological and hydrological droughts using CMIP6 model, Stochastic Environmental Research
633   and Risk Assessment, 36, 3857–3874, 2022.
634 Donat, M. G., Lowry, A. L., Alexander, L. V., O'Gorman, P. A., and Maher, N.: More extreme
635   precipitation in the world's dry and wet regions, Nature Climate Change, 6, 508–513, 2016.
636 Duan, Q., Sorooshian, S., and Gupta, V.: Effective and efficient global optimization for conceptual rainfall-
637   runoff models, , 28, 1015–1031, 1992.
638 Fujimori, S., Hasegawa, T., Masui, T., Takahashi, K., Herran, D. S., Dai, H., Hijioka, Y., and Kainuma, M.:
639   SSP3: AIM implementation of shared socioeconomic pathways, Global Environmental Change, 42,
640   268–283, 2017.
641 Ganguli, P. and Merz, B.: Trends in compound flooding in northwestern Europe during 1901–2014,
642   Geophysical Research Letters, 46, 10810–10820, 2019.
643 Gers, F. A., Schmidhuber, J., and Cummins, F.: Learning to forget: continual prediction with LSTM,
644   Neural Comput, 12, 2451–71, 2000.
645 Green, J. K., Berry, J., Ciais, P., Zhang, Y., and Gentine, P.: Amazon rainforest photosynthesis increases in
646   response to atmospheric dryness, Science Advances, 6, eabb7232, 2020.
647 Gu, L., Chen, J., Yin, J., Sullivan, S. C., Wang, H.-M., Guo, S., Zhang, L., and Kim, J.-S.: Projected
648   increases in magnitude and socioeconomic exposure of global droughts in 1.5 and 2 °C
649   warmer climates, Hydrology and Earth System Sciences, 24, 451–472, https://doi.org/10.5194/hess-
650   24-451-2020, 2020a.
651 Gu, L., Chen, J., Yin, J., Xu, C.-Y., and Zhou, J.: Responses of precipitation and runoff to climate warming
652   and implications for future drought changes in China, Earth's Future, 8, e2020EF001718, 2020b.
653 Gu, L., Yin, J., Zhang, H., Wang, H.-M., Yang, G., and Wu, X.: On future flood magnitudes and estimation
654   uncertainty across 151 catchments in mainland China, International Journal of Climatology, 41, E779–
655   E800, 2021.
656 Gu, L., Yin, J., Wang, S., Chen, J., Qin, H., Yan, X., He, S., and Zhao, T.: How well do the multi-satellite
657   and atmospheric reanalysis products perform in hydrological modelling, Journal of Hydrology, 617,
658   128920, https://doi.org/10.1016/j.jhydrol.2022.128920, 2023.
659 He, B., Lü, A., Wu, J., Zhao, L., and Liu, M.: Drought hazard assessment and spatial characteristics
660   analysis in China, Journal of Geographical Sciences, 21, 235–249, 2011.
661 Hu, C., Guo, S., Xiong, L., and Peng, D.: A modified Xinanjiang model and its application in northern
662   China, Hydrology Research, 36, 175–192, 2005.
663 Jiang, T., Jing, Z., Cheng, J., Lige, C., Yanjun, W., Hemin, S., Anqian, W., Jinlong, H., Buda, S., and Run,
664   W.: National and provincial population projected to 2100 under the shared socioeconomic pathways in
665   China, Advances in Climate Change Research, 13, 128, 2017.
666 Jiang, T., Jing, Z., Li-Ge, C. A. O., Yan-Jun, W., Bu-Da, S. U., Cheng, J., Run, W., and Chao, G. A. O.:
667   Projection of national and provincial economy under the shared socioeconomic pathways in China,
668   Advances in Climate Change Research, 14, 50, 2018.
669 Kim, J. H., Sung, J. H., Chung, E.-S., Kim, S. U., Son, M., and Shiru, M. S.: Comparison of Projection in
670   Meteorological and Hydrological Droughts in the Cheongmicheon Watershed for RCP4. 5 and SSP2-
671   4.5, Sustainability, 13, 2066, 2021.
672 Koutsoyiannis, D.: Clausius–Clapeyron equation and saturation vapour pressure: simple theory reconciled
673   with practice, European Journal of physics, 33, 295, 2012.
674 Kriauciuniene, J., Jakimavicius, D., Sarauskiene, D., and Kaliatka, T.: Estimation of uncertainty sources in
675   the projections of Lithuanian river runoff, Stochastic Environmental Research and Risk Assessment,

676   27, 769–784, 2013.

677   Kumar, R., Musuuza, J. L., Van Loon, A. F., Teuling, A. J., Barthel, R., Ten Broek, J., Mai, J., Samaniego,
678   L., and Attinger, S.: Multiscale evaluation of the Standardized Precipitation Index as a groundwater
679   drought indicator, Hydrology and Earth System Sciences, 20, 1117–1131, 2016.

680   Kundzewicz, Z., Su, B., Wang, Y., Xia, J., Huang, J., and Jiang, T.: Flood risk and its reduction in China,
681   Advances in Water Resources, 130, 37–45, https://doi.org/10.1016/j.advwatres.2019.05.020, 2019.

682   Kunnath-Poovakka, A. and Eldho, T. I.: A comparative study of conceptual rainfall-runoff models GR4J,
683   AWBM and Sacramento at catchments in the upper Godavari river basin, India, J Earth Syst Sci, 128,
684   33, https://doi.org/10.1007/s12040-018-1055-8, 2019.

685   Lange, S.: Trend-preserving bias adjustment and statistical downscaling with ISIMIP3BASD (v1.0),
686   Geoscientific Model Development, 12, 3055–3070, https://doi.org/10.5194/gmd-12-3055-2019, 2019.

687   Li, D. X.: On default correlation: A copula function approach, Available at SSRN 187289,
688   https://doi.org/10.2139/ssrn.187289, 1999.

689   Liu, J., Zhang, Q., Singh, V. P., and Shi, P.: Contribution of multiple climatic variables and human
690   activities to streamflow changes across China, Journal of Hydrology, 545, 145–162,
691   https://doi.org/10.1016/j.jhydrol.2016.12.016, 2017.

692   Liu, Y., Hu, Z.-Z., Wu, R., and Yuan, X.: Causes and predictability of the 2021 spring southwestern China
693   severe drought, Advances in Atmospheric Sciences, 39, 1766–1776, 2022a.

694   Liu, Z., Deng, Z., He, G., Wang, H., Zhang, X., Lin, J., Qi, Y., and Liang, X.: Challenges and opportunities
695   for carbon neutrality in China, Nat Rev Earth Environ, 3, 141–155, https://doi.org/10.1038/s43017-
696   021-00244-x, 2022b.

697   Lu, R., Xu, K., Chen, R., Chen, W., Li, F., and Lv, C.: Heat waves in summer 2022 and increasing concern
698   regarding heat waves in general, Atmospheric and Oceanic Science Letters, 16, 100290,
699   https://doi.org/10.1016/j.aosl.2022.100290, 2023.

700   Ma, N., Szilagyi, J., Zhang, Y., and Liu, W.: Complementary-Relationship-Based Modeling of Terrestrial
701   Evapotranspiration Across China During 1982–2012: Validations and Spatiotemporal Analyses,
702   Journal of Geophysical Research: Atmospheres, 124, 4326–4351,
703   https://doi.org/10.1029/2018JD029850, 2019.

704   Mallapaty, S.: China's extreme weather challenges scientists studying it, Nature, 609, 888, 2022.

705   Martel, J., Demeester, K., Brissette, F., Poulin, A., and Arsenault, R.: HMETS-A simple and efficient
706   hydrology model for teaching hydrological modelling, flow forecasting and climate change impacts,
707   International Journal of Engineering Education, 2017.

708   Meinshausen, M., Nicholls, Z. R., Lewis, J., Gidden, M. J., Vogel, E., Freund, M., Beyerle, U., Gessner, C.,
709   Nauels, A., and Bauer, N.: The shared socio-economic pathway (SSP) greenhouse gas concentrations
710   and their extensions to 2500, Geoscientific Model Development, 13, 3571–3605, 2020.

711   Mokhtar, A., Jalali, M., He, H., Al-Ansari, N., Elbeltagi, A., Alsafadi, K., Abdo, H. G., Sammen, S. S.,
712   Gyasi-Agyei, Y., and Rodrigo-Comino, J.: Estimation of SPEI meteorological drought using machine
713   learning algorithms, IEEE Access, 9, 65503–65523, 2021.

714   Myronidis, D., Ioannou, K., Fotakis, D., and Dörflinger, G.: Streamflow and hydrological drought trend
715   analysis and forecasting in Cyprus, Water resources management, 32, 1759–1776, 2018.

716   Nabaei, S., Sharafati, A., Yaseen, Z. M., and Shahid, S.: Copula based assessment of meteorological
717   drought characteristics: regional investigation of Iran, Agricultural and Forest Meteorology, 276,
718   107611, 2019.

719   Nie, N., Zhang, W., Chen, H., and Guo, H.: A global hydrological drought index dataset based on gravity
720   recovery and climate experiment (GRACE) data, Water Resources Management, 32, 1275–1290,
721   2018.

722   O'Neill, B. C., Tebaldi, C., Van Vuuren, D. P., Eyring, V., Friedlingstein, P., Hurtt, G., Knutti, R.,
723   Kriegler, E., Lamarque, J.-F., and Lowe, J.: The scenario model intercomparison project
724   (ScenarioMIP) for CMIP6, Geoscientific Model Development, 9, 3461–3482, 2016.

725   Oudin, L., Hervieu, F., Michel, C., Perrin, C., Andréassian, V., Anctil, F., and Loumagne, C.: Which
726   potential evapotranspiration input for a lumped rainfall–runoff model?: Part 2—Towards a simple and
727   efficient potential evapotranspiration model for rainfall–runoff modelling, Journal of Hydrology, 303,
728   290–306, 2005.

729   Pelosi, A., Terribile, F., D'Urso, G., and Chirico, G. B.: Comparison of ERA5-Land and UERRA
730   MESCAN-SURFEX reanalysis data with spatially interpolated weather observations for the regional

731   assessment of reference evapotranspiration, Water, 12, 1669, 2020.

732   Perrin, C., Michel, C., and Andréassian, V.: Improvement of a parsimonious model for streamflow
733   simulation, Journal of hydrology, 279, 275–289, 2003.

734   Piao, S., Ciais, P., Huang, Y., Shen, Z., Peng, S., Li, J., Zhou, L., Liu, H., Ma, Y., Ding, Y., Friedlingstein,
735   P., Liu, C., Tan, K., Yu, Y., Zhang, T., and Fang, J.: The impacts of climate change on water resources
736   and agriculture in China, Nature, 467, 43–51, https://doi.org/10.1038/nature09364, 2010.

737   Pokhrel, Y., Felfelani, F., Satoh, Y., Boulange, J., Burek, P., Gädeke, A., Gerten, D., Gosling, S. N.,
738   Grillakis, M., and Gudmundsson, L.: Global terrestrial water storage and drought severity under
739   climate change, Nature Climate Change, 11, 226–233, 2021.

740   Porter, J. W. and McMahon, T. A.: Application of a catchment model in southeastern Australia, Journal of
741   Hydrology, 24, 121–134, 1975.

742   Pörtner, H.-O., Roberts, D. C., Poloczanska, E. S., Mintenbeck, K., Tignor, M., Alegría, A., Craig, M.,
743   Langsdorf, S., Löschke, S., and Möller, V.: IPCC, 2022: Summary for policymakers, 2022.

744   Qi, W., Chen, J., Li, L., Xu, C., Li, J., Xiang, Y., and Zhang, S.: A framework to regionalize conceptual
745   model parameters for global hydrological modeling, Hydrology and Earth System Sciences
746   Discussions, 1–28, https://doi.org/10.5194/hess-2020-127, 2020.

747   Rahmati, O., Falah, F., Dayal, K. S., Deo, R. C., Mohammadi, F., Biggs, T., Moghaddam, D. D., Naghibi,
748   S. A., and Bui, D. T.: Machine learning approaches for spatial modeling of agricultural droughts in the
749   south-east region of Queensland Australia, Science of the Total Environment, 699, 134230, 2020.

750   Ren-Jun, Z.: The Xinanjiang model applied in China, Journal of hydrology, 135, 371–381, 1992.

751   Schmidt, R., Schwintzer, P., Flechtner, F., Reigber, C., Güntner, A., Döll, P., Ramillien, G., Cazenave, A.,
752   Petrovic, S., and Jochmann, H.: GRACE observations of changes in continental water storage, Global
753   and Planetary Change, 50, 112–126, 2006.

754   Sherstinsky, A.: Fundamentals of recurrent neural network (RNN) and long short-term memory (LSTM)
755   network, Physica D: Nonlinear Phenomena, 404, 132306, 2020.

756   Shin, M.-J. and Kim, C.-S.: Component combination test to investigate improvement of the IHACRES and
757   GR4J rainfall–runoff models, Water, 13, 2126, 2021.

758   Shukla, S. and Wood, A. W.: Use of a standardized runoff index for characterizing hydrologic drought,
759   Geophysical research letters, 35, 2008.

760   Simmons, A. J., Untch, A., Jakob, C., Kållberg, P., and Undén, P.: Stratospheric water vapour and tropical
761   tropopause temperatures in Ecmwf analyses and multi-year simulations, , 125, 353–386, 1999.

762   Sohn, J. A., Saha, S., and Bauhus, J.: Potential of forest thinning to mitigate drought stress: A meta-
763   analysis, Forest Ecology and Management, 380, 261–273,
764   https://doi.org/10.1016/j.foreco.2016.07.046, 2016.

765   Sönmez, A. Y. and Kale, S.: Climate change effects on annual streamflow of Filyos River (Turkey),
766   Journal of Water and Climate Change, 11, 420–433, https://doi.org/10.2166/wcc.2018.060, 2018.

767   Stewart, I. T.: Changes in snowpack and snowmelt runoff for key mountain regions, Hydrological
768   Processes, 23, 78–94, https://doi.org/10.1002/hyp.7128, 2009.

769   Tabari, H.: Climate change impact on flood and extreme precipitation increases with water availability,
770   Scientific reports, 10, 1–10, 2020.

771   Tapley, B. D., Bettadpur, S., Ries, J. C., Thompson, P. F., and Watkins, M. M.: GRACE measurements of
772   mass variability in the Earth system, science, 305, 503–505, 2004.

773   Tian, Y., Xu, Y.-P., and Zhang, X.-J.: Assessment of Climate Change Impacts on River High Flows
774   through Comparative Use of GR4J, HBV and Xinanjiang Models, Water Resources Management, 27,
775   2871–2888, 2013.

776   Tirivarombo, S., Osupile, D., and Eliasson, P.: Drought monitoring and analysis: standardised precipitation
777   evapotranspiration index (SPEI) and standardised precipitation index (SPI), Physics and Chemistry of
778   the Earth, Parts A/B/C, 106, 1–10, 2018.

779   Udall, B. and Overpeck, J.: The twenty-first century Colorado River hot drought and implications for the
780   future, Water Resources Research, 53, 2404–2418, 2017.

781   Vicente-Serrano, S. M., López-Moreno, J. I., Beguería, S., Lorenzo-Lacruz, J., Azorin-Molina, C., and
782   Morán-Tejeda, E.: Accurate computation of a streamflow drought index, Journal of Hydrologic
783   Engineering, 17, 318–332, 2012.

784   Wang, Z., Li, J., Lai, C., Zeng, Z., Zhong, R., Chen, X., Zhou, X., and Wang, M.: Does drought in China
785   show a significant decreasing trend from 1961 to 2009?, Science of The Total Environment, 579, 314–

786   324, https://doi.org/10.1016/j.scitotenv.2016.11.098, 2017.
787   Weinfurt, K. P.: Multivariate analysis of variance, in: Reading and understanding multivariate statistics,
788   American Psychological Association, Washington, DC, US, 245–276, 1995.
789   Wilhite, D. A., Svoboda, M. D., and Hayes, M. J.: Understanding the complex impacts of drought: A key to
790   enhancing drought mitigation and preparedness, Water Resour Manage, 21, 763–774,
791   https://doi.org/10.1007/s11269-006-9076-5, 2007.
792   Woolway, R. I., Kraemer, B. M., Lenters, J. D., Merchant, C. J., O'Reilly, C. M., and Sharma, S.: Global
793   lake responses to climate change, Nat Rev Earth Environ, 1, 388–403, https://doi.org/10.1038/s43017-
794   020-0067-5, 2020.
795   Wu, J., Chen, X., Yao, H., and Zhang, D.: Multi-timescale assessment of propagation thresholds from
796   meteorological to hydrological drought, Science of the Total Environment, 765, 144232, 2021.
797   Wu, X., Guo, S., Yin, J., Yang, G., Zhong, Y., and Liu, D.: On the event-based extreme precipitation across
798   China: Time distribution patterns, trends, and return levels, Journal of hydrology, 562, 305–317, 2018.
799   Xiao-jun, W., Jian-yun, Z., Shahid, S., ElMahdi, A., Rui-min, H., Zhen-xin, B., and Ali, M.: Water
800   resources management strategy for adaptation to droughts in China, Mitig Adapt Strateg Glob Change,
801   17, 923–937, https://doi.org/10.1007/s11027-011-9352-4, 2012.
802   Xiujia, C., Guanghua, Y., Jian, G., Ningning, M., and Zihao, W.: Application of WNN-PSO model in
803   drought prediction at crop growth stages: A case study of spring maize in semi-arid regions of
804   northern China, Computers and Electronics in Agriculture, 199, 107155, 2022.
805   Xu, K., Yang, D., Yang, H., Li, Z., Qin, Y., and Shen, Y.: Spatio-temporal variation of drought in China
806   during 1961–2012: A climatic perspective, Journal of Hydrology, 526, 253–264, 2015.
807   Yao, F., Livneh, B., Rajagopalan, B., Wang, J., Crétaux, J.-F., Wada, Y., and Berge-Nguyen, M.: Satellites
808   reveal widespread decline in global lake water storage, Science, 380, 743–749,
809   https://doi.org/10.1126/science.abo2812, 2023.
810   Yevjevich, V. M.: Objective approach to definitions and investigations of continental hydrologic droughts,
811   An, PhD Thesis, Colorado State University. Libraries, 1967.
812   Yihdego, Y., Vaheddoost, B., and Al-Weshah, R. A.: Drought indices and indicators revisited, Arab J
813   Geosci, 12, 69, https://doi.org/10.1007/s12517-019-4237-z, 2019.
814   Yilmaz, M.: Accuracy assessment of temperature trends from ERA5 and ERA5-Land, Science of The Total
815   Environment, 856, 159182, https://doi.org/10.1016/j.scitotenv.2022.159182, 2023.
816   Yin, J., Guo, S., He, S., Guo, J., Hong, X., and Liu, Z.: A copula-based analysis of projected climate
817   changes to bivariate flood quantiles, Journal of hydrology, 566, 23–42, 2018.
818   Yin, J., Guo, S., Gu, L., He, S., Ba, H., Tian, J., Li, Q., and Chen, J.: Projected changes of bivariate flood
819   quantiles and estimation uncertainty based on multi-model ensembles over China, Journal of
820   Hydrology, 585, 124760, 2020.
821   Yin, J., Guo, S., Gu, L., Zeng, Z., Liu, D., Chen, J., Shen, Y., and Xu, C.-Y.: Blending multi-satellite,
822   atmospheric reanalysis and gauge precipitation products to facilitate hydrological modelling, Journal
823   of Hydrology, 593, 125878, 2021a.
824   Yin, J., Guo, S., Gentine, P., Sullivan, S. C., Gu, L., He, S., Chen, J., and Liu, P.: Does the hook structure
825   constrain future flood intensification under anthropogenic climate warming?, Water Resources
826   Research, 57, e2020WR028491, 2021b.
827   Yin, J., Guo, S., Yang, Y., Chen, J., Gu, L., Wang, J., He, S., Wu, B., and Xiong, J.: Projection of droughts
828   and their socioeconomic exposures based on terrestrial water storage anomaly over China, Sci. China
829   Earth Sci., 65, 1772–1787, https://doi.org/10.1007/s11430-021-9927-x, 2022.
830   Yin, J., Gentine, P., Slater, L., Gu, L., Pokhrel, Y., Hanasaki, N., Guo, S., Xiong, L., and Schlenker, W.:
831   Future socio-ecosystem productivity threatened by compound drought–heatwave events, Nat Sustain,
832   6, 259–272, https://doi.org/10.1038/s41893-022-01024-1, 2023.
833   Yu, B. and Zhu, Z.: A comparative assessment of AWBM and SimHyd for forested watersheds,
834   Hydrological sciences journal, 60, 1200–1212, 2015.
835   Yu, Y., Si, X., Hu, C., and Zhang, J.: A Review of Recurrent Neural Networks: LSTM Cells and Network
836   Architectures, Neural Comput, 31, 1235–1270, 2019.
837   Zhai, P. M. and Zou, X. K.: Changes in temperature and precipitation and their impacts on drought in
838   China during 1951–2003, Advances in Climate Change Research, 1, 16–18, 2005.
839   Zhang, F., Deng, X., Xie, L., and Xu, N.: China's energy-related carbon emissions projections for the
840   shared socioeconomic pathways, Resources, Conservation and Recycling, 168, 105456, 2021.

841   Zhang, G., Gan, T. Y., and Su, X.: Twenty-first century drought analysis across China under climate
842   change, Climate Dynamics, 59, 1665–1685, 2022.
843   Zhao, M., A, G., Velicogna, I., and Kimball, J. S.: Satellite Observations of Regional Drought Severity in
844   the Continental United States Using GRACE-Based Terrestrial Water Storage Changes, Journal of
845   Climate, 30, 6297–6308, https://doi.org/10.1175/JCLI-D-16-0458.1, 2017.
846   Zheng, J., Wang, H., and Liu, B.: Impact of the long-term precipitation and land use changes on runoff
847   variations in a humid subtropical river basin of China, Journal of Hydrology: Regional Studies, 42,
848   101136, 2022.
849   Zhu, Q., Luo, Y., Zhou, D., Xu, Y.-P., Wang, G., and Tian, Y.: Drought prediction using in situ and remote
850   sensing products with SVM over the Xiang River Basin, China, Natural Hazards, 105, 2161–2185,
851   2021.
852